



**HAL**  
open science

## Investigating the role of evaporation in dew formation under different climates using 17O-excess

Chao Tian, Wenzhe Jiao, Daniel Beysens, Kudzai Farai Kaseke,  
Marie-Gabrielle Medici, Fadong Li, Lixin Wang

### ► To cite this version:

Chao Tian, Wenzhe Jiao, Daniel Beysens, Kudzai Farai Kaseke, Marie-Gabrielle Medici, et al.. Investigating the role of evaporation in dew formation under different climates using 17O-excess. *Journal of Hydrology*, 2021, 592, pp.125847. 10.1016/j.jhydrol.2020.125847 . hal-04005207

**HAL Id: hal-04005207**

**<https://hal.science/hal-04005207>**

Submitted on 19 Mar 2023

**HAL** is a multi-disciplinary open access archive for the deposit and dissemination of scientific research documents, whether they are published or not. The documents may come from teaching and research institutions in France or abroad, or from public or private research centers.

L'archive ouverte pluridisciplinaire **HAL**, est destinée au dépôt et à la diffusion de documents scientifiques de niveau recherche, publiés ou non, émanant des établissements d'enseignement et de recherche français ou étrangers, des laboratoires publics ou privés.



28 **Abstract**

29 With increasing aridity in many regions, dew is likely to play an increasingly important role in  
30 the ecohydrological processes in many ecosystems, especially in arid and semiarid regions. Few  
31 studies investigated the role of evaporation during dew formation and how it varies under  
32 different climate settings.  $^{17}\text{O}$ -excess, as a new tracer, could be used to extract information of  
33 evaporation dynamics from natural water samples (e.g., precipitation, river, and lake). Therefore,  
34 to fill the knowledge gap in evaporation mechanisms during dew formation, we report the  
35 isotopic variation ( $\delta^2\text{H}$ ,  $\delta^{18}\text{O}$ ,  $\delta^{17}\text{O}$ , and  $^{17}\text{O}$ -excess) of dew and precipitation from three distinct  
36 climatic regions (i.e., Gobabeb in the central Namib Desert, Nice in France with Mediterranean  
37 climate, and Indianapolis in the central United States with humid continental climate). We  
38 examined whether dew formed in different climate settings was affected by different degree of  
39 evaporation using observed isotopic values and evaporation models during the formation  
40 processes, and modeled the effects of key meteorological variables (i.e., temperature and relative  
41 humidity) on  $^{17}\text{O}$ -excess variations. The results showed that dew in Gobabeb experienced kinetic  
42 fractionation associated with evaporation under non-steady state conditions during dew  
43 formation with enriched  $\delta^{18}\text{O}$  and low  $^{17}\text{O}$ -excess values. Dew formations with temperatures  
44 over  $14.7^\circ\text{C}$  in Indianapolis were also influenced by evaporation under non-steady state  
45 conditions. However, dew formation in Nice did not experience significant evaporation.  
46 Evaporation processes (equilibrium or kinetic fractionation) occurring during nights with heavy  
47 dew under three climate settings were mainly related to the variation of atmosphere relative  
48 humidity. The  $^{17}\text{O}$ -excess tracer provides a new method to distinguish the different evaporation  
49 processes (equilibrium or kinetic fractionation) during dew formation and our result provides an  
50 improved understanding of dew formation.

51 **Keywords:** drylands; ecohydrology; equilibrium fractionation; kinetic fractionation; stable  
52 isotopes

53

## 54 **1. Introduction**

55 Dew is the condensation of water vapor into liquid droplets on a substrate when the  
56 substrate surface temperature drops below the dew point (Beysens, 2018; Monteith and  
57 Unsworth, 2013). It usually occurs at night or in early morning when reduced input of shortwave  
58 radiation results in a negative net radiation balance at the substrate. Dew occurs in most climate  
59 zones. It is an important source of moisture for epiphytes and lichens with special physical  
60 features absorbing atmospheric moisture (Gerlein-Safdi et al., 2018). Dew can reach and even  
61 exceed annual rainfall and serve as a sustainable and stable water source to maintain plant and  
62 small animal survival in arid and semiarid environments (Kidron et al., 2011; Tomaszkiwicz et  
63 al., 2015; Wang et al., 2017), especially during periods of drought. Dew could even be the only  
64 water source in a continental semiarid grassland (Aguirre-Gutiérrez et al., 2019). It is also  
65 viewed as a small but important part of the water balance in humid areas (Ritter et al., 2019;  
66 Tuller and Chilton, 1973). Dew significantly increased soil water potential such as in Namib  
67 Desert (Wang et al., 2019). It can be directly absorbed by plant roots from soil, and can reduce  
68 the evaporation loss of soil moisture to mediate water status in water-stressed plants (Aguirre-  
69 Gutiérrez et al., 2019; Munné-Bosch and Alegre, 1999). As a water source, dew can also be  
70 directly absorbed through leaves, and then alter leaf-level energy balance, reduce transpiration  
71 rate, and improve photosynthesis (Grammatikopoulos and Manetas, 1994; Guo et al., 2016; Rao  
72 et al., 2009; Zhang et al., 2019).

73 Air temperature and relative humidity (RH), the environmental determinants of dew  
74 deposition, are expected to change rapidly with climate change, and may affect the frequency  
75 and amount of dew deposition (Cook et al., 2014; Nepstad et al., 2008; Tomaszekiewicz et al.,  
76 2016; Vuollekoski et al., 2015). Previous studies showed that nocturnal temperatures increase  
77 with climate change, implying a lower RH and lower dew amounts in the future (Donat and  
78 Alexander, 2012; Martín et al., 2012). In a continental-scale study, it is found that the frequency  
79 of dew formation at night in the grasslands is between 15% and 95% during the study period and  
80 dew formation has a strong linear relationship with nocturnal RH (Ritter et al., 2019). Generally,  
81 when dew forms, the RH of ambient air should be high enough (>70%), and the substrate surface  
82 temperature should drop below the dew point due to radiative cooling (Lekouch et al., 2010).  
83 However, recent study showed that dew may form at lower RH as long as vapor saturation occur  
84 at the air-substrate interface (Kidron and Starinsky, 2019). For instance, a study in the semi-arid  
85 region of Loess Plateau of China indicated that dew can form when RH is around 30% (Wang  
86 and Zhang, 2011). Therefore, RH controls on dew formation may differ among climate regions.  
87 Most previous research does not consider evaporation during dew formation because it occurs  
88 during night or in early morning and evaporation is considered minimum. As a result, the role of  
89 evaporation during dew formation is not well understood. However, evaporation during dew  
90 formation has been observed in the past. For instance, evaporation during dew formation is  
91 observed during 2:00 to 4:00 am in the Loess Plateau of China leading to a decreasing dew  
92 amount (Wang and Zhang, 2011). It is also observed in Linze inland river basin (Fang and Ding,  
93 2005). The knowledge gaps in dew evaporation during formation hinder our understanding of  
94 dew formation mechanisms and an accurate prediction of dew formation changes under future  
95 climates. Although the dew amount collected (traditional method) at sequential times at night or

96 in early morning can be used to indicate evaporation process, continuous dew recording is  
97 logistically challenging and difficult to implement due to intensive labor requirement.

98 Stable isotopes of traditional hydrogen and oxygen ( $\delta^2\text{H}$  and  $\delta^{18}\text{O}$ ) are natural tracers to  
99 diagnose changes in different hydrometeorological processes undergoing equilibrium and kinetic  
100 fractionation during water phase change (Crawford et al., 2013; Cui et al., 2020; Soderberg et al.,  
101 2012; Zhao et al., 2012). The equilibrium fractionation is determined by the saturation vapor  
102 pressure. The kinetic fractionation is attributed to different diffusivities of different isotopes.  
103 Generally, dew is one type of liquid condensation, supposedly dominated by equilibrium  
104 fractionation. To the best of our knowledge, there is no effort examining the two fractionation  
105 processes (equilibrium and kinetic fractionation) associated with evaporation during dew  
106 formation. Condensation can be considered as the inverse of evaporation, with similar  
107 fractionation mechanisms between vapor and liquid. As such, isotope studies on dew  
108 condensation mechanism can be used to better understand the two fractionation processes  
109 associated with evaporation during dew formation process. For instance, the  $\delta^{18}\text{O}$  values in  
110 surface dew in Brazil consistently tracked atmospheric vapor  $\delta^{18}\text{O}$  values, which is generally  
111 regarded as the Rayleigh equilibrium fractionation process (Zhang et al., 2009). Wen et al. (2012)  
112 point out that the effect of equilibrium fractionation on the  $\delta^2\text{H}$  and  $\delta^{18}\text{O}$  of dew is greater than  
113 that of the kinetic fractionation although humidity deviated from the saturation conditions by up  
114 to 120% on the leaf surface in a cropland and a grassland in China. Deshpande et al. (2013)  
115 recognize that dew could involve a certain degree of kinetic fractionation in super-saturated  
116 environments at a coastal village of India. These dew formation studies, based on  $\delta^2\text{H}$  and  $\delta^{18}\text{O}$ ,  
117 can distinguish equilibrium and kinetic fractionation processes. However, these studies are either  
118 based on the assumption of equilibrium fractionation during condensation (Zhang et al., 2009) or

119 require measuring atmospheric water vapor isotopes and dew isotopes simultaneously  
120 (Deshpande et al., 2013; Wen et al., 2012).

121 Recent advance in spectroscopy have now enabled to obtain high-precision measurements  
122 of  $\delta^{17}\text{O}$  with low natural abundance. A new hydrological tracer  $^{17}\text{O}$ -excess became available to  
123 provide additional constraints on the mechanisms of water phase changes (Barkan and Luz,  
124 2007). The major advantage of  $^{17}\text{O}$ -excess over the conventional isotopes is its sole RH  
125 dependence between 10°C to 45°C (Barkan and Luz, 2005; Cao and Liu, 2011), which is  
126 confirmed by field observations (Landais et al., 2010; Li et al., 2017; Uechi and Uemura, 2019;  
127 Winkler et al., 2012). Recent studies also show that the relationship between  $\delta^{18}\text{O}$  and  $\delta^{17}\text{O}$  can  
128 be used to better reveal tap water and precipitation formation mechanisms (Tian et al., 2020;  
129 Tian et al., 2019), differentiate synoptic drought and local drought (Kaseke et al., 2018), and  
130 distinguish fog and dew (Kaseke et al., 2017).

131 According to the conceptual evaporation model,  $^{17}\text{O}$ -excess and the relationships between  
132 different isotopic parameters (e.g.,  $\delta^{18}\text{O}$  vs.  $\delta^{17}\text{O}$ ;  $^{17}\text{O}$ -excess vs.  $\delta^{18}\text{O}$  (or d-excess)) can be  
133 used to infer whether water is affected by equilibrium fractionation or kinetic fractionation  
134 associated with evaporation under steady state or non-steady state (Barkan and Luz, 2005;  
135 Barkan and Luz, 2007; Criss, 1999). The evaporation model under steady state condition was  
136 based on traditional Rayleigh fractionation model. Rayleigh distillation assumes that water vapor  
137 evaporates in isotopic equilibrium condition with no additional sources or vapor recycling  
138 processes (e.g., evaporative recharge or atmospheric transport characteristics) (Fiorella et al.,  
139 2019; Winnick et al., 2014). However, most natural evaporation under non-steady state condition  
140 depends on external atmospheric vapor. Therefore, the significant difference of boundary  
141 conditions between steady-state and non-steady state models is the existence of atmospheric

142 water vapor, resulting in differently shaped evaporation trajectories (Li et al., 2015). The  
143 relationships between different isotopic parameters have been used to estimate precipitation  
144 evaporation processes in Africa and in the central U.S. (Landais et al., 2010; Tian et al., 2018).  
145 The relationships have also been used to analyze evaporation loss of natural water bodies in the  
146 Sistan Oasis, Iran (Surma et al., 2015), in central Atacama Desert, Chile (Surma et al., 2018),  
147 and in western U.S. (Passey and Ji, 2019). Overall,  $^{17}\text{O}$ -excess and the relationships between  
148 different isotopic parameters are effective to explore the detailed evaporation processes.

149 Dew research has been largely confined to arid and semiarid environments (Beysens, 2018;  
150 Tomaszekiewicz et al., 2015; Uclés et al., 2015). Therefore, a large knowledge gap exists to study  
151 dew variability among different climatic regions (e.g., arid and humid regions in the inland and  
152 near ocean) especially for evaporation. It is important to understand the environmental factors  
153 influencing dew formation in different climate regions and this will better inform us how these  
154 factors will affect dew formation under climate change. Here, we investigate dew and  
155 precipitation isotopic variations to explore the evaporation mechanisms of dew formation in  
156 three different climate settings including Gobabeb Research and Training Center (hereafter  
157 Gobabeb) in the central Namib Desert with desert climate, Nice in France with Mediterranean  
158 climate, and Indianapolis in the central United States with humid continental climate. We used  
159  $^{17}\text{O}$ -excess and the relationships between  $\delta^{18}\text{O}$  and  $\delta^{17}\text{O}$  as well as between  $^{17}\text{O}$ -excess and  
160  $\delta^{18}\text{O}$  (or d-excess) to characterize evaporation dynamics under different climate settings and  
161 examined the influence of meteorological factors (e.g., temperature and RH) on isotopes.  
162 Additionally, two evaporation models under steady state (i.e., Rayleigh model) and non-steady  
163 state conditions were also used to verify whether dew was affected by evaporation during its  
164 formation. Furthermore, the sensitivity of temperature and RH, the two important meteorological

165 parameters in evaporation model and the most susceptible to climate change, were also analyzed  
166 to examine their influence on dew evaporation processes under various environmental conditions.

## 167 **2. Material and methods**

### 168 **2.1. Site description**

169 This study was conducted in different climatic regions (Table 1). Gobabeb Research and  
170 Training Center (23.55° S, 15.04° E; 405 m above sea level) is located about 60 km from the  
171 South Atlantic Ocean on the outer edge of the central Namib Desert in Namibia. The mean  
172 annual temperature and mean annual relative humidity are 21.1°C and 50%, respectively (Qiao et  
173 al., 2020). The annual precipitation amount is less than 20 mm (Kaseke et al., 2017). Nice  
174 (43.74° N, 7.27° E; 310 m above sea level) in France is situated between the Mediterranean Sea  
175 and the Alps mountains. It is Mediterranean climate associated with hot, dry summers and mild,  
176 wet winters. The minimum and maximum of average monthly temperature are 12.4°C in January  
177 and 19.6°C in August, respectively, with an annual average of 16.0°C, based on meteorological  
178 data from 1981 to 2010 (<http://www.meteofrance.com/climat/france/nice/06088001/normales>).  
179 The variations of average monthly RH are from 75% in February to 80% in May, with an annual  
180 average of 78%. The mean annual precipitation is 733 mm, with over 75% of the precipitation  
181 occurring between October and the following April. Both Gobabeb and Nice are close to the  
182 ocean. Indianapolis (39.88° N, 86.27° W; 258 m above sea level) is an inland city in the Midwest  
183 of the United States. Detailed meteorological characteristics in Indianapolis have been described  
184 in our previous study (Tian et al., 2018). In brief, mean annual temperature, mean annual relative  
185 humidity, and precipitation are 10.2°C, 69%, and 953 mm, respectively  
186 (<https://www.wunderground.com>). To evaluate the degree of dryness in the three sites, aridity  
187 index values were extracted from the Global Aridity Index dataset

188 (<https://cgiarcsi.community/data/global-aridity-and-pet-database/>). The Gobabeb was hyper-arid  
189 site with aridity index of 0.01. The Nice and Indianapolis were both humid sites with aridity  
190 index of 0.98 and 0.96, respectively. According to the Köppen climate classification (Geiger,  
191 1961; Köppen, 1936), the climate in Gobabeb, Nice, and Indianapolis belongs to desert climate,  
192 Mediterranean climate, and humid continental climate, respectively.

## 193 **2.2. Sample collections and isotope analysis**

194 Event-based dew and precipitation samples were collected at each site. To reduce  
195 evaporation effects on isotopes, all of dew samples were collected before dawn at each site and  
196 stored in sealed glass vials (15 ml) for the samples in Gobabeb and Indianapolis or polyethylene  
197 bottles for the dew samples in Nice. All of the precipitation samples were collected immediately  
198 after each event or at the earliest possible time in the morning if the precipitation event was  
199 finished after midnight. Twenty-two dew samples were collected from July 2014 to June 2017 in  
200 Gobabeb. Five rainfall samples were collected in January, February, September 2014, and  
201 February 2016. Four shallow groundwaters and two deep groundwaters were also collected.  
202 Twenty-three dew samples were collected in Nice from December 2017 to April 2018. Sixty-  
203 nine dew samples and 109 precipitation samples (including 99 rainfalls and 10 snowfalls) were  
204 collected in Indianapolis from January 2017 to October 2017 and throughout 2017, respectively.  
205 All dew and precipitation samples were delivered to the IUPUI Ecohydrology Lab to measure  
206 isotopic variations using a Triple Water Vapor Isotope Analyzer (T-WVIA-45-EP; Los Gatos  
207 Research Inc. (LGR), Mountain View, CA, USA) coupled to a Water Vapor Isotope Standard  
208 Source (WVISS, LGR, Mountain View, CA, USA). The detailed operation and calibration  
209 procedures were described in details by Tian et al. (2016) and Wang et al. (2009). The main  
210 isotopic parameters reported here are:  $\delta^{18}\text{O} = 1000 \times \ln(\delta^{18}\text{O} + 1)$ ,  $\delta^{17}\text{O} = 1000 \times \ln(\delta^{17}\text{O} + 1)$ ,  $\lambda$

211  $= \delta^{18}\text{O}/\delta^{17}\text{O}$ ,  $^{17}\text{O}$ -excess =  $\ln(\delta^{17}\text{O} + 1) - 0.528 \times \ln(\delta^{18}\text{O} + 1)$ , d-excess =  $\delta^2\text{H} - 8 \times \delta^{18}\text{O}$   
212 (Barkan and Luz, 2007; Meijer and Li, 1998). Additionally, all of the isotope ratios were  
213 normalized using two international water standards (Vienna Standard Mean Ocean Water  
214 (VSMOW) and Standard Light Antarctic Precipitation (SLAP)) following the procedure  
215 described by Steig et al. (2014) and Schoenemann et al. (2013). Furthermore, to ensure the  
216 accuracy of  $^{17}\text{O}$ -excess measurements,  $^{17}\text{O}$ -excess values were filtered through the methods of  
217 Tian et al. (Tian and Wang, 2019; Tian et al., 2018). Based on the detection criterion, the  
218 precision of our instrument was  $<0.80\text{‰}$ ,  $<0.06\text{‰}$ ,  $<0.03\text{‰}$ , and  $<12$  per meg (1 per meg =  
219  $0.001\text{‰}$ ) for  $\delta^2\text{H}$ ,  $\delta^{18}\text{O}$ ,  $\delta^{17}\text{O}$ , and  $^{17}\text{O}$ -excess, respectively, which was comparable with previous  
220 studies (Berman et al., 2013; Luz and Barkan, 2010; Schoenemann et al., 2013; Steig et al.,  
221 2014).

### 222 **2.3. Meteorological variables**

223 To examine dew formation mechanisms under different climate settings, nocturnal  
224 temperature and RH were used for analysis associated with  $^{17}\text{O}$ -excess variations. The  
225 meteorological data were available at the different meteorological stations: Gobabeb:  
226 <http://www.sasscalweathernet.org/>; Nice: <https://www.infoclimat.fr/>;  
227 Indianapolis: <https://www.wunderground.com>. The download date was about October 26<sup>th</sup>,  
228 November 30<sup>th</sup>, and October 23<sup>th</sup> in 2018 for the above three websites, respectively. The  
229 nocturnal data in this study were screened and averaged to hourly data from 12:00 am to 6:00 am.

### 230 **2.4. Evaporation model description**

231 To examine whether dew under different climate settings are affected by evaporation during  
232 formation, two types of evaporation models (steady state and non-steady state conditions) were  
233 used in this study. Simulated isotopic values were compared with the measured values. If most of

234 the simulated isotopic values matched with the measured values at temperature and RH  
 235 conditions close to the measurements, the model was considered as the optimal one. The choice  
 236 of steady state or non-steady state evaporation model was also verified by the observed  
 237 relationships between  $\delta^{18}\text{O}$  and  $\delta^{17}\text{O}$  as well as between  $^{17}\text{O}$ -excess and  $\delta^{18}\text{O}$  (or d-excess).

#### 238 *2.4.1. Evaporation simulation without external moisture sources*

239 The atomic ratio of the residual water  $^*\text{R}_{\text{end}}$  under steady state condition can be calculated  
 240 by the Rayleigh fractionation model as a function of  $^*\alpha_{\text{evap}}$  (Criss, 1999).

$$241 \quad ^*\text{R}_{\text{end}} = ^*\text{R}_{\text{start}} f^{(1/^*\alpha_{\text{evap}}-1)} \quad , \quad (1)$$

242 where  $^*\text{R}_{\text{end}}$  and  $^*\text{R}_{\text{start}}$  are the isotopic ratios ( $\text{H}_2^{17}\text{O}/\text{H}_2^{16}\text{O}$  or  $\text{H}_2^{18}\text{O}/\text{H}_2^{16}\text{O}$ ) of the residual water  
 243 and initial water, respectively.  $f$  is the residual fraction of liquid water.  $^*\alpha_{\text{evap}}$  is evaporation  
 244 fractionation factor, a function of the RH during evaporation process (Barkan and Luz, 2007).

$$245 \quad ^*\alpha_{\text{evap}} = ^*\text{R}_W/^*\text{R}_E = \frac{^*\alpha_{\text{diff}} ^*\alpha_{\text{eq}} (1-\text{RH})}{1-^*\alpha_{\text{eq}}\text{RH}(^*\text{R}_A/^*\text{R}_W)} \quad , \quad (2)$$

246 where  $^*\alpha_{\text{eq}}$  and  $^*\alpha_{\text{diff}}$  are liquid-vapor equilibrium fractionation factor and the diffusion  
 247 fractionation factor for  $^{17}\text{O}/^{16}\text{O}$  or  $^{18}\text{O}/^{16}\text{O}$ , respectively.  $\text{R}_W$ ,  $\text{R}_E$ , and  $\text{R}_A$  are the isotopic ratios of  
 248 liquid, evaporating water, and air moisture, respectively. Under the steady state experimental  
 249 setup, all of the water vapor comes from the evaporating water body (i.e., no external moisture  
 250 source), which means  $\text{R}_A = \text{R}_E$ . Therefore, the above equation (2) can be simplified to (Barkan  
 251 and Luz, 2007):

$$252 \quad ^*\alpha_{\text{evap}} = ^*\alpha_{\text{eq}}(^*\alpha_{\text{diff}}(1 - \text{RH}) + \text{RH}) \quad , \quad (3)$$

253  $^{18}\alpha_{\text{eq}}$  and  $^{17}\alpha_{\text{eq}}$  are controlled by temperature (Horita and Wesolowski, 1994):

$$254 \quad ^{18}\alpha_{\text{eq}} = \exp[(-7.685 + (6.7123(10^3/T)) - (1.6664(10^6/T^2)) + (0.35041(10^9/T^3)))/10^3] \quad , \quad (4)$$

255  ${}^2\alpha_{\text{eq}} =$   
 256  $\exp[(1158.8(T^3/10^9) - 1620.1(T^2/10^6) + 794.84(T/10^3) - 161.04 +$   
 257  $2.9992(10^9/T^3))/10^3]$ . (5)

258  ${}^{17}\alpha_{\text{eq}}$  was estimated using  ${}^{17}\alpha_{\text{eq}} = ({}^{18}\alpha_{\text{eq}})^{0.529}$  based on liquid-vapor equilibrium experiments  
 259 (Barkan and Luz, 2005). The  ${}^{18}\alpha_{\text{diff}}$  was 1.0283, and  ${}^{17}\alpha_{\text{diff}}$  was  $({}^{18}\alpha_{\text{diff}})^{0.518}$  based on molecular  
 260 diffusivities of water vapor in air during evaporation experiments (Barkan and Luz, 2007).  ${}^2\alpha_{\text{diff}}$   
 261 was estimated using  ${}^2\alpha_{\text{diff}} = ({}^{18}\alpha_{\text{diff}})^{0.88}$  from Merlivat (1978) and confirmed by Luz et al. (2009).  
 262 Therefore, in our study, the  ${}^{18}\alpha_{\text{diff}}$ ,  ${}^2\alpha_{\text{diff}}$ , and  ${}^{17}\alpha_{\text{diff}}$  were 1.0283, 1.02486, and 1.01456,  
 263 respectively.

#### 264 **2.4.2. Evaporation simulation with external moisture sources**

265 The isotopic ratios of residual water ( ${}^*\mathbf{R}_w$ ) under non-steady state condition can be  
 266 calculated by the following equation (6) (Criss, 1999):

267 
$${}^*\mathbf{R}_w = f^u ({}^*\mathbf{R}_w^i - {}^*\mathbf{R}_w^s) + {}^*\mathbf{R}_w^s, \quad (6)$$

268 where  $f$  is the residual fraction of liquid water; the exponent  $u$  is the fractionation factor as a  
 269 function of RH:

270 
$$u = \frac{1 - {}^*\alpha_{\text{evap}}^0 (1 - \text{RH})}{{}^*\alpha_{\text{evap}}^0 (1 - \text{RH})}, \quad (7)$$

271 where  ${}^*\alpha_{\text{evap}}^0$  is the effective evaporation fractionation factor at 0% RH, which could be  
 272 calculated by equation (2).  ${}^*\mathbf{R}_w^i$  is the isotopic ratio of initial water.  ${}^*\mathbf{R}_w^s$  is the predicted isotopic  
 273 ratio of residual water under steady exchange with atmospheric vapor ( ${}^*\mathbf{R}_v$ ).

274 
$${}^*\mathbf{R}_w^s = \frac{{}^*\alpha_{\text{eq}} \text{RH} {}^*\mathbf{R}_v}{1 - {}^*\alpha_{\text{evap}}^0 (1 - \text{RH})}. \quad (8)$$

275  $^*R_v$  was not directly measured in our study. It was determined either from literature value or  
 276 calculated using precipitation isotopic composition and the equilibrium fractionation factor  
 277 between liquid and vapor, as shown in equation (9) (Barkan and Luz, 2005).

$$278 \quad ^*\alpha_{l/v} = \frac{(\delta^{18}O_l + 1)}{(\delta^{18}O_v + 1)}, \quad (9)$$

279 where  $^*\alpha_{l/v}$  is a temperature-dependent equilibrium fractionation factor, calculated by the equation  
 280 (4) and (5).  $\delta^{18}O = (^*R_s/^*R_{ref} - 1)$ , and  $^*R_s$  and  $^*R_{ref}$  are the isotope ratios (e.g.,  $^{18}O/^{16}O$  or  $^{17}O/^{16}O$ ) of  
 281 the sample and reference, respectively.

282 According to the relationships between  $\delta^{18}O$  and  $\delta^{17}O$  as well as between  $^{17}O$ -excess and  
 283  $\delta^{18}O$  (or d-excess), all of the dew in Gobabeb and some of the dew in Indianapolis were affected  
 284 by evaporation, while those in Nice were not affected by evaporation. The evaporated dew in  
 285 Indianapolis were the dew that occurred when the temperature was greater than  $14.7^\circ C$  (thirty-  
 286 three events, hereafter the dew $_{T \geq 14.7^\circ C}$ ). As for the dew $_{T \geq 14.7^\circ C}$ , there were significant relationships  
 287 between  $^{17}O$ -excess and  $\delta^{18}O$  (or d-excess) with higher correlation coefficients ( $r = -0.54$  (or  
 288  $0.48$ );  $p < 0.01$ ) than the ones under lower temperature. Therefore, dew in Gobabeb and  
 289 Indianapolis were simulated separately using the above two evaporation models under steady  
 290 state and non-steady state conditions, while the dew evaporation in Nice was not simulated. For  
 291 each evaporation model, different boundary conditions (including different variables and  
 292 parameters) were simulated to search for the optimal model in terms of temperature, RH, residual  
 293 fraction of liquid water ( $f$ ), and isotopic values of both initial water (i.e.,  $^*R_{start}$  or  $^*R_w^i$  for steady  
 294 state or non-steady state) and atmospheric water vapor ( $^*R_v$ ). Different models of dew were  
 295 simulated through fixed mean nocturnal temperature parameter and adjusted RH during the  
 296 observation period. If the adjusted RH value was close to the observed mean RH value,  
 297 corresponding to the similarity between the simulated and observed isotopic values including

298 relationships between  $\delta^{18}\text{O}$  and  $\delta^{17}\text{O}$  as well as between  $^{17}\text{O}$ -excess and  $\delta^{18}\text{O}$  (or d-excess), the  
299 model would be considered as the optimal one.

300 Generally, isotopic value of the initial water in the model was the minimum value of all the  
301 observed values for one particular site (e.g., dew in Gobabeb under non-steady state condition)  
302 (Table 2). However, not all models followed the above criterion because some dew with  
303 minimum values might not be affected by evaporation. If the ideal model cannot be obtained  
304 using the minimum value, the relatively low value will be considered as isotopic value of the  
305 initial water (e.g., dew<sub>T $\geq$ 14.7 $^{\circ}$ C</sub> in Indianapolis under non-steady state condition). With the  
306 decreasing of residual fraction of liquid water (f), the evaporation processes increased associated  
307 with the enriched  $\delta^{18}\text{O}$  and decreasing  $^{17}\text{O}$ -excess, which means that f also played an important  
308 role in simulating evaporation. The equilibrium fractionation factors ( $\alpha_{\text{eq}}$ ) were calculated by  
309 equation (4) and (5) using average nocturnal temperature (and not daily temperature as  
310 mentioned later on) because dew occurs at night.

311 The isotopic value of atmospheric water vapor was another important variable in non-steady  
312 state model. The data can be deduced from previous study (e.g., dew in Gobabeb) (Uemura et al.,  
313 2010). They can also be calculated by the equilibrium relationship between precipitation and  
314 water vapor following equation (9) due to the lack of direct observational vapor data. The  
315 equilibrium relationship has been applied in previous studies, such as for a prolonged rain event  
316 and for monthly precipitation in Beijing, China (Wen et al., 2010). Fiorella et al. (2019) also  
317 point out that the equilibrium assumption gives relatively accurate estimates of the isotope ratios  
318 of evaporating waters in low latitudes (equatorward of 30 $^{\circ}$ ). It is noteworthy that to obtain the  
319 isotopic values of water vapor, compared with using average nocturnal temperature as mentioned  
320 above, the average daily temperature was used to calculate the equilibrium fractionation factor

321 ( $\alpha_{l/v}$ ) as shown in Table 2. This is because the process of converting precipitation into water  
322 vapor occurs during both day and night. For the isotopic values of precipitation, some of them  
323 were from the directly collected samples, and others were from empirical Online Isotopes in  
324 Precipitation Calculator (hereafter OIPC) model. Both of them were used to calculate the water  
325 vapor to further obtain optimal models in Gobabeb and Indianapolis. The  $^{17}\text{O}$ -excess of local  
326 atmospheric vapor was assumed to be 33 per meg based on the global meteoric water (Luz and  
327 Barkan, 2010) because the OIPC data only include  $\delta^2\text{H}$  and  $\delta^{18}\text{O}$ . Additionally, for dew in  
328 Gobabeb, the mean isotopic values of measured meteoric water included not only local rainfall  
329 but also the shallow groundwater and deep groundwater.

## 330 **2.5. Temperature and RH sensitivity analysis**

331 To further explore the role of temperature and RH on  $^{17}\text{O}$ -excess variations of dew, we used  
332 the evaporation model under non-steady state mentioned above to simulate the effects of  
333 temperature and RH on  $^{17}\text{O}$ -excess in Gobabeb and Indianapolis (only dew $_{T \geq 14.7^\circ\text{C}}$  was used for  
334 the Indianapolis site since they are affected by evaporation).

335 For the sensitivity of temperature, for both of the sites, the temperature from  $1.4^\circ\text{C}$  (the  
336 minimum nocturnal value) to  $30.0^\circ\text{C}$  including the maximum nocturnal value ( $21.4^\circ\text{C}$ ) were used  
337 to include all of the conditions for dew formation. For each site, the average nocturnal  
338 temperature and the observed minimum and maximum values for dew were also simulated to test  
339 the temperature sensitivity. For the sensitivity of RH, RH ranging from 18% to 98% with every  
340 10% interval was used in the two sites, which include the optimal RH 78% in Gobabeb and 98%  
341 in Indianapolis as stated in the above optimal model. The other boundary conditions were  
342 assumed constant by using parameters (e.g.,  $R_w^i$ ,  $R_v$ , and  $f$ ) from the optimal model.

343

### 344 3. Results

#### 345 3.1. Meteorological characteristics of dew days

346 There were different nocturnal temperature and RH ranges under three different climate  
347 settings during the observation periods (Fig. 1). The average temperature in Nice was the lowest  
348 (9.1°C) with the smallest range (3.6°C to 15.3°C), and the average in Indianapolis was the  
349 highest (13.9°C) with the largest range (1.4°C to 21.4°C). The temperature in Gobabeb varied  
350 from 3.5°C to 16.9°C with an average of 11.8°C. It is notable that the average RH in Gobabeb  
351 was the lowest (78%) with the largest range values (35% to 98%), and the average in  
352 Indianapolis was the highest (92%) with the smallest range values (66% to 100%). The RH in  
353 Nice varied from 55% to 94% with an average of 80%. Additionally, for the days with  
354  $dew_{T \geq 14.7^\circ C}$  in Indianapolis, the temperature varied from 14.7°C to 21.4°C with an average of  
355 17.4°C, and the RH varied from 66% to 99% with an average of 93%.

#### 356 3.2. Dew isotope variations

357 A largest range of dew  $\delta^{18}O$  values was observed in Nice during the study period (-16.7‰  
358 to -0.7‰) (Fig. 2). It was close to the range in Indianapolis (-13.4‰ to 0.5‰), while the smallest  
359 range was in Gobabeb (-6.8‰ to 3.2‰). The average  $\delta^{18}O$  value in Gobabeb was more enriched  
360 (-1.4‰±2.6‰) than the other two sites. The average  $\delta^{18}O$  value in Nice (-7.0‰±3.8‰) was  
361 almost similar to the one in Indianapolis (-6.5‰±3.1‰), while lower than those for the  
362  $dew_{T \geq 14.7^\circ C}$  in Indianapolis (-5.1‰±2.6‰). The  $\delta^2H$  and  $\delta^{17}O$  variations showed similar trends to  
363  $\delta^{18}O$  in the three sites (Fig. 2).

364 More variable dew  $^{17}O$ -excess values were observed in Gobabeb (-40 to 45 per meg) (Fig.  
365 2). The range in Nice (7 to 54 per meg) was close to the one in Indianapolis (-5 to 64 per meg).  
366 The average  $^{17}O$ -excess value in Gobabeb (9±22 per meg) was the lowest, and the one in Nice

367 (34±12 per meg) was almost identical to the ones in Indianapolis for all dew events (35±11 per  
368 meg) and for dews with dew<sub>T≥14.7°C</sub> (34±14 per meg) (Fig. 2). The largest range of d-excess  
369 values was observed in Gobabeb (-19.9‰ to 26.5‰), and the smallest range was in Nice (0.1‰  
370 to 32.3‰) (Fig. 2). The range in Indianapolis was from -5.0‰ to 32.1‰. The average d-excess  
371 value in Gobabeb was the lowest (6.4‰±10.0‰). The average in Nice was the highest  
372 (18.1‰±8.8‰). The average for all dew events and for dew<sub>T≥14.7°C</sub> in Indianapolis were  
373 12.7‰±7.2‰ and 10.3‰±5.6‰, respectively.

374 The slope of  $\delta^{18}\text{O}-\delta^{17}\text{O}$  ( $\lambda$ ) in Gobabeb (0.5202) was smaller than that in Nice and  
375 Indianapolis (0.5268 and 0.5271) (Fig. 3). The slope of all the samples in the three sites was  
376 0.5253. The  $^{17}\text{O}$ -excess was negatively correlated with  $\delta^{18}\text{O}$  in Gobabeb ( $r = -0.93$ ,  $p < 0.001$ )  
377 and for all the samples ( $r = -0.61$ ,  $p < 0.001$ ) (Fig. 4a). The  $^{17}\text{O}$ -excess was positively correlated  
378 with d-excess ( $r = 0.74$ ,  $p < 0.001$ ) and the slope between  $^{17}\text{O}$ -excess and d-excess was 1.61 per  
379 meg/‰ in Gobabeb (Fig. 4b). The  $^{17}\text{O}$ -excess was positively correlated with d-excess ( $r = 0.50$ ,  $p$   
380  $< 0.001$ ) and the slope between  $^{17}\text{O}$ -excess and d-excess was 0.96 per meg/‰ for all the samples.  
381 There was no relationship between  $^{17}\text{O}$ -excess and  $\delta^{18}\text{O}$  (or d-excess) in Nice ( $p > 0.05$ ). For all  
382 dew events in Indianapolis, there was a low negative correlation between  $^{17}\text{O}$ -excess and  $\delta^{18}\text{O}$  ( $r$   
383  $= -0.25$ ,  $p = 0.037$ ). To probe dew evaporation in Indianapolis, dew occurring under different  
384 temperature groups were used to analyze their relationships among different isotopic variables.  
385 The results showed that  $\lambda$  for the dew<sub>T≥14.7°C</sub> was 0.5252. The  $^{17}\text{O}$ -excess was negatively  
386 correlated with  $\delta^{18}\text{O}$  ( $r = -0.54$ ,  $p = 0.001$ ) and positively correlated with d-excess ( $r = 0.48$ ,  $p =$   
387  $0.004$ ) associated with a slope of 1.18 per meg/‰ (Fig. 5c-d). Dew with temperature below  
388 14.7°C had the higher  $\lambda$  (0.5280), and there was no correlation between  $^{17}\text{O}$ -excess and  $\delta^{18}\text{O}$  (or  
389 d-excess) ( $p > 0.05$ ).

390 In order to further reveal the dew formation mechanisms, the relationships between the  $^{17}\text{O}$ -  
391 excess and both temperature and RH were analyzed in the three sites and for all the samples. The  
392 results showed that there was no relationship between temperature and  $^{17}\text{O}$ -excess, while positive  
393 correlation was observed between RH and  $^{17}\text{O}$ -excess for all of the samples ( $r = 0.34$ ,  $p < 0.001$ )  
394 (Fig. 6). Therefore, the difference in dew  $^{17}\text{O}$ -excess among the three sites was mainly driven by  
395 RH differences.

### 396 **3.3. Dew evaporation simulation**

397 Hundreds of dew evaporation simulations were conducted under various boundary  
398 conditions in Gobabeb and Indianapolis under steady state and non-steady state conditions. The  
399 optimal evaporation models in Gobabeb and in Indianapolis for the  $\text{dew}_{T \geq 14.7^\circ\text{C}}$  were both  
400 attained under non-steady state condition. The detailed variables and parameters are shown in  
401 Table 2. Note that the isotopic values of atmospheric water vapor were both calculated on the  
402 basis of the equilibrium fractionation between precipitation and vapor (Barkan and Luz, 2005).  
403 As for dew in Gobabeb, the  $\delta^{18}\text{O}$ ,  $\delta^{17}\text{O}$ ,  $\delta^2\text{H}$ , and  $^{17}\text{O}$ -excess of vapor were  $-13.305\%$ ,  $-7.047\%$ ,  
404  $-102.898\%$ , and 0 per meg, respectively. These values produced better simulation results than  
405 those from the directly observed vapor data from the South Indian and the Southern Oceans ( $-$   
406  $15.5 \pm 2.7\%$ ,  $-8.2 \pm 1.5\%$ , and 16 per meg for  $\delta^{18}\text{O}$ ,  $\delta^{17}\text{O}$ , and  $^{17}\text{O}$ -excess, respectively) (Uemura et  
407 al., 2010). For precipitation in Gobabeb, comparing with the isotopic values from empirical  
408 Online Isotopes in Precipitation Calculator model ( $-2.6 \pm 0.4\%$  and  $-13 \pm 4\%$  for  $\delta^{18}\text{O}$  and  $\delta^2\text{H}$ ,  
409 respectively), the mean isotopic values of measured local precipitation (including rainfall and  
410 groundwater;  $-3.5 \pm 6.0\%$  and  $-25.7 \pm 41.7\%$  for  $\delta^{18}\text{O}$  and  $\delta^2\text{H}$ , respectively) were used to estimate  
411  $\delta^{18}\text{O}_v$  and  $\delta^2\text{H}_v$  because it could get a better match with measured values in the model. As a result,  
412 the temperature and RH of optimal model for dew in Gobabeb were identical with those of the

413 measured average nocturnal values during the observation period (11.8°C and 78%). The  
414 simulated  $\lambda$  (0.5199) was almost the same with the observed  $\lambda$  (0.5202) (Fig. 5a-b). The negative  
415 correlations between  $^{17}\text{O}$ -excess and  $\delta^{18}\text{O}$  were similar for simulated and measured values (slope  
416 = -8.10 and -7.76 per meg/‰ for both) (Fig. 5a). The positive correlation between  $^{17}\text{O}$ -excess  
417 and d-excess for the model (slope = 1.58 per meg/‰) was similar with the observed value (1.61  
418 per meg/‰) (Fig. 5b).

419 As for the dew<sub>T $\geq$ 14.7°C</sub> in Indianapolis, the  $\delta^{18}\text{O}$ ,  $\delta^{17}\text{O}$ ,  $\delta^2\text{H}$ , and  $^{17}\text{O}$ -excess of the vapor were  
420 -14.950‰, -7.902‰, -109.725‰, and 20 per meg, respectively. The isotopic values of  
421 precipitation were from the observed value during dew observation (-5.25‰ and -33.79‰ for  
422  $\delta^{18}\text{O}$  and  $\delta^2\text{H}$ ). Using the observed precipitation values could get better simulated values than  
423 using the OIPC values (-3.20‰ and -15.40‰). With these parameters (Table 2), RH of optimal  
424 model in Indianapolis (98%) was found close to the measured average nocturnal values (93%)  
425 (Fig. 5c-d). The modeled  $\lambda$  (0.5250) was close to the observed one (0.5252). The negative  
426 correlations between  $^{17}\text{O}$ -excess and  $\delta^{18}\text{O}$  were similar for simulated and measured values (slope  
427 = -3.01 and -2.84 per meg/‰ for both) (Fig. 5c). The positive correlation between  $^{17}\text{O}$ -excess  
428 and d-excess for the model (slope = 1.17 per meg/‰) was almost identical to the observed value  
429 (slope = 1.18 per meg/‰) (Fig. 5d).

### 430 **3.4. The sensitivity of temperature and RH on dew $^{17}\text{O}$ -excess**

431 In order to assess the dew  $^{17}\text{O}$ -excess sensitivity to temperature and RH, the evaporation  
432 models mentioned above were also used to simulate the dew  $^{17}\text{O}$ -excess responses to different  
433 environmental conditions in Gobabeb and Indianapolis. The dew  $^{17}\text{O}$ -excess sensitivity with  
434 respect to temperature and RH is shown in Fig. 7. The results indicated the  $^{17}\text{O}$ -excess were more  
435 sensitive to changes in RH regardless the formation sites. For instance, for dew in Gobabeb,

436 negative correlations were observed between  $^{17}\text{O}$ -excess and  $\delta^{18}\text{O}$  modeled by the non-steady  
437 evaporation model. The values of  $\lambda$  (0.5183 to 0.5208) varied slightly with large changes in  
438 temperature (1.4°C to 30.0°C) when RH was 78% (the optimal model parameter). However, the  $\lambda$   
439 values (0.5187 to 0.5252) changed more significantly with large changes in RH (18% to 98%)  
440 when temperature was 11.8°C (the average value during the study period) (Fig. 7a-b). Similarly,  
441 for the  $\text{dew}_{T \geq 14.7^\circ\text{C}}$  in Indianapolis,  $\lambda$  only varied from 0.5238 to 0.5260 with large changes in  
442 temperature (1.4°C to 30.0°C) when RH was 98%, while  $\lambda$  varied from 0.5227 to 0.5255 with  
443 large changes in RH (18% to 98%) when temperature was 17.4°C (Fig. 7c-d). It was worth  
444 noting that  $\lambda$  decreased with increasing temperature (1.4°C to 30.0°C) for dew in Gobabeb and  
445 Indianapolis with  $\text{dew}_{T \geq 14.7^\circ\text{C}}$ , while there was no significant linear relationship between  $\lambda$  and  
446 RH regardless the dew formation sites.

447

## 448 **4. Discussion**

### 449 **4.1. Dew evaporation mechanisms**

450 Dew is recognized as an important contribution to the annual water balance in arid and  
451 semiarid ecosystems (Aguirre-Gutiérrez et al., 2019; Kidron et al., 2011; Tomaszekiewicz et al.,  
452 2015; Wang et al., 2017) even in humid region (Ritter et al., 2019; Tuller and Chilton, 1973).  
453 The importance of dew may be magnified in arid regions to alleviate water stress on natural  
454 ecosystems under changing climate (Rahimi et al., 2013). Dew formation obeys relatively  
455 complex phase change processes in different environments. In reality, dew formation does not  
456 always occur within a short time window but often lasts for several hours during the night or in  
457 early morning. Dew is often collected before dawn for many dew researches, but evaporation is  
458 likely to be unavoidable during dew formation. Evaporation can occur when the conditions for  
459 dew formation are not fulfilled any more, e.g., with lower relative humidity, which decreases the

460 dew point temperature with respect to air temperature, during wind gusts where heat exchange  
461 with air is enhanced, or rise of cloud cover, decreasing radiative cooling. In the previous studies  
462 on dew evaporation, the different fractionation processes (equilibrium or kinetic fractionation)  
463 are speculated based on the dew isotopic variations of condensation since evaporation and  
464 condensation are inverse phase-change processes (Deshpande et al., 2013; Wen et al., 2012).  
465 However, these studies did not provide direct evidence of different fractionation processes due to  
466 the lack of real-time monitoring of vapor isotopic variation. In addition, because real-time  
467 monitoring of vapor isotopic variation needs intensive labor and other logistics (e.g., instrument  
468 purchase, deployment, and power consumption), it is difficult to test dew formation mechanism  
469 at long-time scale and no research has been conducted to examine the different degrees of  
470 evaporation. In the current study, to alleviate these constraints, we used  $^{17}\text{O}$ -excess and its  
471 relationships with other isotopic parameters (e.g.,  $\delta^{18}\text{O}$  vs.  $\delta^{17}\text{O}$ ;  $^{17}\text{O}$ -excess vs.  $\delta^{18}\text{O}$  (or d-  
472 excess)) to probe whether dew is affected by equilibrium fractionation or kinetic fractionation  
473 associated with evaporation using dew from three distinct climate settings.

474 The largest range of dew  $^{17}\text{O}$ -excess values was observed in arid Gobabeb with lowest  
475 average  $^{17}\text{O}$ -excess value ( $9\pm 22$  per meg) and the most enriched  $\delta^{18}\text{O}$  value ( $-1.4\%\pm 2.6\%$ ) than  
476 observed in other two humid regions in Nice and Indianapolis (Fig. 2). The  $\lambda$  value (0.5202) was  
477 the lowest in Gobabeb, which was close to the diffusive fractionation of atmospheric water vapor  
478 (0.5185) (Barkan and Luz, 2007) and close to previous study result at the same site (0.516)  
479 (Kaseke et al., 2017). There were significant correlations between  $^{17}\text{O}$ -excess and both  $\delta^{18}\text{O}$  and  
480 d-excess in Gobabeb. The slope between  $^{17}\text{O}$ -excess and d-excess in Gobabeb (1.61 per meg/ $\%$ )  
481 is similar to the values predicted by re-evaporation model in African monsoon rainfall (1.6 to 2.0  
482 per meg/ $\%$ ) (Landais et al., 2010). These indicated that the dew in Gobabeb might be more

483 susceptible to kinetic fractionation associated with evaporation at non-steady state than the other  
484 two humid regions in Nice and Indianapolis, which exerts a stronger impact on the isotopic  
485 exchange process leading to the more enriched  $\delta^{18}\text{O}$  values and lower  $^{17}\text{O}$ -excess values for  
486 Gobabeb dew. This has been confirmed by the detailed evaporation modeling as described in  
487 section 4.2 (Fig. 5).

488 The  $\lambda$  value of dew in Nice (0.5268) is close to the equilibrium fractionation exponent  
489 (0.529) of the liquid-vapor equilibrium and global meteoric water line (0.528) (Barkan and Luz,  
490 2005; Luz and Barkan, 2010). It appears that Rayleigh distillation, which usually limits to the  
491 equilibrium processes, was the main mechanism explaining the temporal variations in the dew  
492 isotope values (Li et al., 2015; Wen et al., 2010).

493 For the dew $_{T\geq 14.7^\circ\text{C}}$  in Indianapolis, the positive correlation between  $^{17}\text{O}$ -excess and  $\delta^{18}\text{O}$   
494 and the negative correlation between  $^{17}\text{O}$ -excess and d-excess (1.18 per meg/‰) was comparable  
495 with the results of tap water in the United States (0.7 to 2.0 per meg/‰) (Li et al., 2015).  
496 Additionally, the  $\lambda$  value (0.5252) of the dew $_{T\geq 14.7^\circ\text{C}}$  was lower than the equilibrium fractionation  
497 exponent (0.529), with relatively high RH (93%). According to the evaporation models  
498 mentioned by Li et al. (2015), if the evaporation process occurred under steady state with high  
499 RH, the  $\lambda$  would be high and close to the equilibrium fractionation exponent. This demonstrated  
500 that the dew $_{T\geq 14.7^\circ\text{C}}$  in Indianapolis likely go through evaporation at non-steady state conditions,  
501 which is consistent with the theoretical evaporation model predictions as further discussed below.

## 502 **4.2. Data-evaporation model comparison**

503 To validate whether dew is influenced by evaporation as expected with  $^{17}\text{O}$ -excess and  $\delta^{18}\text{O}$   
504 observations, two evaporation models under steady state based on Rayleigh model and non-  
505 steady state model were used to reproduce the observed results, which reflects different degrees

506 of equilibrium or kinetic fractionation associated with evaporation. To evaluate the quality of  
507 model fitting, a series of the evaporation-controlled evolution of  $^{17}\text{O}$ -excess over  $\delta^{18}\text{O}$  (or d-  
508 excess) had been simulated with variable boundary conditions.

509 In our study, dew in Gobabeb and the dew $_{T \geq 14.7^\circ\text{C}}$  in Indianapolis both experienced kinetic  
510 fractionation associated with evaporation under non-steady state condition. The initial water  
511 isotopic values were the observed minimum isotopic values in Gobabeb, while they were not the  
512 minimum values in Indianapolis. These indicated that all of the dew samples in Gobabeb could  
513 be included in the evaporation model and were susceptible to the evaporation, while not all of the  
514 dew $_{T \geq 14.7^\circ\text{C}}$  in Indianapolis were affected by evaporation. Compared with simulated values under  
515 Rayleigh evaporation process, isotopic variation of residual water was significantly enriched  
516 during kinetic fractionation associated with evaporation process under non-steady state  
517 conditions. As for dew in Gobabeb, the observed  $\delta^{18}\text{O}$  and  $\delta^{17}\text{O}$  values were better matched with  
518 the simulated values under non-steady state than those under steady state. To facilitate the  
519 comparison with previous studies, the slope between  $^{17}\text{O}$ -excess and d-excess (or  $\delta^{18}\text{O}$ ) for the  
520 observed and simulated dew in Gobabeb were calculated based on linear correlations, although  
521 the significance of quadratic relationship between  $^{17}\text{O}$ -excess and d-excess was a little higher  
522 than that of the linear relationship. The similar positive correlation between  $^{17}\text{O}$ -excess and d-  
523 excess for the model and the observed value (1.58 per meg/‰ vs. 1.61 per meg/‰) indicated that  
524 the isotopic variations of dew in Gobabeb should mainly occur under non-steady state  
525 evaporation condition.

526  $^{17}\text{O}$ -excess of water vapor in the optimal model in Gobabeb was 0 per meg as calculated from  
527 the relationship between  $\delta^{17}\text{O}$  and  $\delta^{18}\text{O}$ . This is a value that fits better with the observed data  
528 than using the mean value of global meteoric water 33 per meg (Luz and Barkan, 2010), which is

529 commonly used when direct observational data are lacking (e.g., in the Sistan Oasis, Iran (Surma  
530 et al., 2015) and in central Atacama Desert, Chile (Surma et al., 2018)). Note that our study is the  
531 first to use the calculated  $^{17}\text{O}$ -excess values of water vapor to predict the evaporation model. It  
532 demonstrates that the mean value of global meteoric waters does not apply anywhere, especially  
533 in arid region where other water resources other than precipitation (e.g., groundwater) have also  
534 an important impact on the local water cycle. The optimal model temperature and RH values in  
535 Gobabeb are found identical to the mean nocturnal temperature and RH during the observation  
536 period (11.8°C and 78%).

537 As for the  $\text{dew}_{T \geq 14.7^\circ\text{C}}$  in Indianapolis, the optimal simulated  $\delta^{18}\text{O}$  and  $\delta^{17}\text{O}$  values under  
538 non-steady state condition are closer to the observation than those under steady state, resulting in  
539 a simulated  $\lambda$  (0.5250) similar to the observed value (0.5252) (Fig. 5c-d), thus suggesting that  
540 evaporation under non-steady state condition is more appropriate during the study period. The  
541 positive relationship between  $^{17}\text{O}$ -excess and d-excess of the optimal model closely coincides  
542 with the measured relationship (slopes 1.17 per meg/‰ vs. 1.18 per meg/‰) (Fig. 5d), which  
543 indicates that  $\text{dew}_{T \geq 14.7^\circ\text{C}}$  in Indianapolis with high RH (93%) experiences a certain degree of  
544 evaporation at non-steady state condition. Therefore, if RH is close to saturation (i.e., for nearly  
545 saturated air 100% relative humidity) and  $\lambda$  not close to the equilibrium fractionation exponent  
546 (0.529), the evaporation process is more likely to occur under non-steady state. This means that  
547 if there are two evaporation processes with same RH, the lower  $\lambda$  indicates that water is more  
548 susceptible to evaporation under non-steady state, a result also verified by the evaporation  
549 processes of tap waters in the U.S. (Li et al., 2015).

550 During the process of evaporation simulation for the  $\text{dew}_{T \geq 14.7^\circ\text{C}}$  in Indianapolis, the isotopic  
551 values of atmospheric water vapor, without direct measurements, were also inferred based on the

552 assumption that vapor and precipitation condensation is an equilibrium fractionation process  
553 (Barkan and Luz, 2005). For the isotopic values of precipitation, the precipitation events between  
554 May and September were selected and their mean value was calculated because the dew<sub>T $\geq$ 14.7 $^{\circ}$ C</sub>  
555 mainly occurred during the period. The isotopic values of the measured precipitations were lower  
556 than those from the OIPC model and could give better prediction. Additionally, the <sup>17</sup>O-excess of  
557 water vapor in optimal model in Indianapolis was 20 per meg, which is a better value than using  
558 the mean value of global meteoric waters 33 per meg (Luz and Barkan, 2010). This further  
559 provides data on water vapor isotopes in Indianapolis during May and September. In  
560 consequence, the RH of optimal model in Indianapolis (98%) was close to the observed average  
561 nocturnal value (93%), which indicates that the optimal model at non-steady state condition can  
562 basically simulate the observed values. The reason is that, during the late spring, summer, and  
563 early fall, long nights and high temperature with low RH, makes evaporation more likely to  
564 occur.

#### 565 **4.3. Sensitivity of temperature and RH**

566 Although dew formation is included in many global climate models (Rosenzweig and  
567 Abramopoulos, 1997), the role of evaporation during dew formation in different climatic regions,  
568 especially under climate change, is not well understood. The isotope evaporation models include  
569 two important meteorological parameters: temperature and RH, and both are changing rapidly  
570 under climate change with increasing temperature and decreasing RH. Lower air temperature and  
571 higher RH are favorable meteorological conditions for the formation of dew (Beysens, 1995; Li,  
572 2002; Ye et al., 2007). But the sensitivity of the effects of temperature and RH on evaporation  
573 processes (indicated by <sup>17</sup>O-excess) during the dew formation is not clear. To this end, the <sup>17</sup>O-  
574 excess sensitivity analysis to temperature and RH were performed based on the different

575 evaporation processes under non-steady state conditions in Gobabeb and Indianapolis with the  
576  $dew_{T \geq 14.7^\circ C}$ . The evaporation lines curved under non-steady states in both Gobabeb and  
577 Indianapolis (Fig. 7). For the sensitivity of temperature, the range of slope  $\lambda$  varied slightly by  
578 0.0025 and 0.0022 in Gobabeb and Indianapolis, respectively. There were negative relationships  
579 between temperature and  $\lambda$  at both sites. The evaporation lines at both sites were clustered  
580 together and changes slightly with the increasing of temperature from 1.4°C to 30°C at the two  
581 sites. These indicated that the  $^{17}O$ -excess and  $\delta^{18}O$  were less sensitive to temperature (from  
582 1.4°C to 30°C), especially for  $^{17}O$ -excess variations, which were also observed for groundwater  
583 evaporation with no detectable change in  $^{17}O$ -excess from 18°C to 28°C in central Atacama  
584 Desert, Chile (Surma et al., 2018). Surma et al. (2015) also showed that air temperature (from  
585 10°C to 30°C) play a minor role for the isotopic composition of evaporating water of natural  
586 water bodies in the Sistan Oasis, Iran. Notably, all of the  $\lambda$  (ranging from 0.5183 to 0.5208) in  
587 Gobabeb were the low, close to the diffusion fractionation (kinetic) factor for water vapor (0.518)  
588 (Barkan and Luz, 2007). However, the  $\lambda$  in Indianapolis (ranging from 0.5238 to 0.5260) were  
589 higher and had less departure from the global meteoric waters line (0.528) (Luz and Barkan,  
590 2010) and equilibrium fractionation factor for water (0.529) (Barkan and Luz, 2005). The  
591 difference is possibly due to RH difference (78% vs. 98% at two sites). This indirectly confirms  
592 the importance of the RH in evaporation as further discussed below in the sensitivity analysis.

593 Concerning the sensitivity of RH (from 18% to 98%) under fixed temperature, with the  
594 decreasing of RH, evaporation curves tend to be more stretched (Fig. 7). This is similar to what  
595 was observed for groundwater evaporation in central Atacama Desert, Chile (RH from 25% to  
596 65%) (Surma et al., 2018). The slope  $\lambda$  range of simulated dew varied widely by 0.0065 and  
597 0.0028 for the two sites. These demonstrated that the dew  $^{17}O$ -excess values were more sensitive

598 to the changes in RH than that in temperature regardless the location. This strengthened the view  
599 that  $^{17}\text{O}$ -excess is principally influenced by RH during  $10^{\circ}\text{C}$  to  $45^{\circ}\text{C}$ , which has been confirmed  
600 by theoretical experiments (Barkan and Luz, 2005; Cao and Liu, 2011) and previous field  
601 observations (Landais et al., 2010; Li et al., 2017; Uechi and Uemura, 2019; Winkler et al.,  
602 2012). Meanwhile, this confirms that RH is the principal drivers of dew formation in the  
603 evaporation model under non-steady state. Furthermore, the  $^{17}\text{O}$ -excess for all of the dew data in  
604 our study was positively correlated with RH, which is consistent with the observations in Africa  
605 monsoon rainfall (Landais et al., 2010). However,  $^{17}\text{O}$ -excess has no relationship with  
606 temperature, meaning that the local RH exerts an important influence on  $^{17}\text{O}$ -excess during dew  
607 evaporation under the different climate settings.

## 608 **5. Conclusions**

609 Dew plays an increasing important role in the ecohydrological processes in many  
610 ecosystems especially under climate change. The present report is the first to study and analyze  
611 whether dew is influenced by different degree of evaporation by means of  $^{17}\text{O}$ -excess and the  
612 relationships between different isotopic parameters (e.g.,  $\delta^{18}\text{O}$  vs.  $\delta^{17}\text{O}$ ;  $^{17}\text{O}$ -excess vs.  $\delta^{18}\text{O}$  (or  
613 d-excess)). The study has been carried out in three different sites with various climate settings  
614 (Gobabeb: desert climate, Nice: Mediterranean climate, and Indianapolis: humid continental  
615 climate). Mean value  $^{17}\text{O}$ -excess of dew in hyper-arid Gobabeb ( $9\pm 22$  per meg) was the lowest  
616 with the largest range, while they were similar in other two humid regions Nice ( $34\pm 12$  per meg)  
617 and Indianapolis ( $35\pm 11$  per meg). Based on observed data and simulations, we conclude that  
618 dew formation in Gobabeb experienced kinetic fractionation processes associated with  
619 evaporation under non-steady state, as well as for some of the dew events with temperature over  
620  $14.7^{\circ}\text{C}$  in Indianapolis, while the dew formation in Nice did not experience significant

621 evaporation. The local RH difference is responsible for the evaporation difference (equilibrium  
622 or kinetic fractionation) of dew formation, which is also supported by the sensitivity analysis.  
623 Informed by these results,  $^{17}\text{O}$ -excess can be considered as a useful tracer to reveal the different  
624 evaporation process (equilibrium or kinetic fractionation) during dew formation under different  
625 climate settings.

626

### 627 **Acknowledgements**

628 This study was supported by the Indiana University-Purdue University Indianapolis  
629 Research Support Funds Grant, the President's International Research Awards from Indiana  
630 University, U.S. National Science Foundation (EAR-1554894), and the National Science  
631 Foundation of China (42007155). We would like to thank two anonymous reviewers for their  
632 constructive comments and suggestions, which we believe significantly strengthened our  
633 manuscript.

634 **REFERENCE**

- 635 Aguirre-Gutiérrez, C.A., Holwerda, F., Goldsmith, G.R., Delgado, J., Yopez, E., Carbajal, N., Escoto-  
636 Rodríguez, M., Arredondo, J.T., 2019. The importance of dew in the water balance of a  
637 continental semiarid grassland. *Journal of Arid Environments*, 168: 26-35.
- 638 Barkan, E., Luz, B., 2005. High precision measurements of  $^{17}\text{O}/^{16}\text{O}$  and  $^{18}\text{O}/^{16}\text{O}$  ratios in  $\text{H}_2\text{O}$ . *Rapid*  
639 *Communications in Mass Spectrometry*, 19(24): 3737-3742.
- 640 Barkan, E., Luz, B., 2007. Diffusivity fractionations of  $\text{H}_2^{16}\text{O}/\text{H}_2^{17}\text{O}$  and  $\text{H}_2^{16}\text{O}/\text{H}_2^{18}\text{O}$  in air and their  
641 implications for isotope hydrology. *Rapid Commun. Mass Spectrom.*, 21(18): 2999-3005.
- 642 Berman, E.S., Levin, N.E., Landais, A., Li, S., Owano, T., 2013. Measurement of  $\delta^{18}\text{O}$ ,  $\delta^{17}\text{O}$  and  $^{17}\text{O}$ -excess  
643 in water by Off-Axis Integrated Cavity Output Spectroscopy and Isotope Ratio Mass  
644 Spectrometry. *Anal. Chem.*, 85(21): 10392-10398.
- 645 Beysens, D., 1995. The formation of dew. *Atmos. Res.*, 39(1-3): 215-237.
- 646 Beysens, D., 2018. *Dew Water*. River Publishers.
- 647 Cao, X., Liu, Y., 2011. Equilibrium mass-dependent fractionation relationships for triple oxygen isotopes.  
648 *Geochim. Cosmochim. Acta*, 75(23): 7435-7445.
- 649 Cook, B.I., Smerdon, J.E., Seager, R., Coats, S., 2014. Global warming and 21 st century drying. *Clim. Dyn.*,  
650 43(9-10): 2607-2627.
- 651 Crawford, J., Hughes, C.E., Parkes, S.D., 2013. Is the isotopic composition of event based precipitation  
652 driven by moisture source or synoptic scale weather in the Sydney Basin, Australia? *Journal of*  
653 *Hydrology*, 507: 213-226.
- 654 Criss, R.E., 1999. *Principles of stable isotope distribution*. Oxford University Press on Demand.
- 655 Cui, J., Tian, L., Wei, Z., Huntingford, C., Wang, P., Cai, Z., Ma, N., Wang, L., 2020. Quantifying the  
656 controls on evapotranspiration partitioning in the highest alpine meadow ecosystems. *Water*  
657 *Resour. Res.* <https://doi.org/10.1029/2019WR024815>.
- 658 Deshpande, R., Maurya, A., Kumar, B., Sarkar, A., Gupta, S., 2013. Kinetic fractionation of water isotopes  
659 during liquid condensation under super-saturated condition. *Geochimica et Cosmochimica Acta*,  
660 100: 60-72.
- 661 Donat, M.G., Alexander, L.V., 2012. The shifting probability distribution of global daytime and night-time  
662 temperatures. *Geophys. Res. Lett.*, 39(14).
- 663 Fang, J., Ding, Y., 2005. Study of the condensation water and its effect factors on the Fringes of Desert  
664 Oasis. *J. Glaciol. Geocryol.*, 27(5): 755-760.
- 665 Fiorella, R.P., West, J.B., Bowen, G.J., 2019. Biased estimates of the isotope ratios of steady-state  
666 evaporation from the assumption of equilibrium between vapour and precipitation. *Hydrol.*  
667 *Process.*: 1-15.
- 668 Geiger, R., 1961. *berarbeitete Neuauflage von Geiger, R: Köppen-Geiger/Klima der Erde. Wandkarte*  
669 *(wall map)*, 1: 16.
- 670 Gerlein-Safdi, C., Koochafkan, M.C., Chung, M., Rockwell, F.E., Thompson, S., Caylor, K.K., 2018. Dew  
671 deposition suppresses transpiration and carbon uptake in leaves. *Agricultural and Forest*  
672 *Meteorology*, 259: 305-316.
- 673 Grammatikopoulos, G., Manetas, Y., 1994. Direct absorption of water by hairy leaves of *Phlomis*  
674 *fruticosa* and its contribution to drought avoidance. *Canadian Journal of Botany*, 72(12): 1805-  
675 1811.
- 676 Guo, X., Zha, T., Jia, X., Wu, B., Feng, W., Xie, J., Gong, J., Zhang, Y., Peltola, H., 2016. Dynamics of Dew in  
677 a Cold Desert-Shrub Ecosystem and Its Abiotic Controls. *Atmosphere*, 7(3): 32.
- 678 Horita, J., Wesolowski, D.J., 1994. Liquid-vapor fractionation of oxygen and hydrogen isotopes of water  
679 from the freezing to the critical temperature. *Geochimica et Cosmochimica Acta*, 58(16): 3425-  
680 3437.

681 Kaseke, K.F., Wang, L., Seely, M.K., 2017. Nonrainfall water origins and formation mechanisms. *Sci. adv.*,  
682 3(3): e1603131.

683 Kaseke, K.F., Wang, L., Wanke, H., Tian, C., Lanning, M., Jiao, W., 2018. Precipitation origins and key  
684 drivers of precipitation isotope ( $^{18}\text{O}$ ,  $2\text{H}$ , and  $^{17}\text{O}$ ) compositions over Windhoek. *Journal of*  
685 *Geophysical Research: Atmospheres*, 123(14): 7311-7330.

686 Kidron, G.J., Starinsky, A., 2019. Measurements and ecological implications of non-rainfall water in  
687 desert ecosystems—A Review. *Ecohydrology*: e2121.

688 Kidron, G.J., Temina, M., Starinsky, A., 2011. An investigation of the role of water (rain and dew) in  
689 controlling the growth form of lichens on cobbles in the Negev Desert. *Geomicrobiology Journal*,  
690 28(4): 335-346.

691 Koppen, W., 1936. Das geographische system der klimat. *Handbuch der klimatologie*: 46.

692 Landais, A., Risi, C., Bony, S., Vimeux, F., Descroix, L., Falourd, S., Bouygues, A., 2010. Combined  
693 measurements of  $^{17}\text{O}$ -excess and d-excess in African monsoon precipitation: Implications for  
694 evaluating convective parameterizations. *Earth Planet. Sci. Lett.*, 298(1): 104-112.

695 Lekouch, I., Mileta, M., Muselli, M., Milimouk-Melnytchouk, I., Šojat, V., Kabbachi, B., Beysens, D., 2010.  
696 Comparative chemical analysis of dew and rain water. *Atmos. Res.*, 95(2-3): 224-234.

697 Li, S., Levin, N.E., Chesson, L.A., 2015. Continental scale variation in  $^{17}\text{O}$ -excess of meteoric waters in the  
698 United States. *Geochim. Cosmochim. Acta*, 164: 110-126.

699 Li, S., Levin, N.E., Soderberg, K., Dennis, K.J., Caylor, K.K., 2017. Triple oxygen isotope composition of leaf  
700 waters in Mpala, central Kenya. *Earth and Planetary Science Letters*, 468: 38-50.

701 Li, X., 2002. Effects of gravel and sand mulches on dew deposition in the semiarid region of China. *J.*  
702 *Hydrol.*, 260(1-4): 151-160.

703 Luz, B., Barkan, E., 2010. Variations of  $^{17}\text{O}/^{16}\text{O}$  and  $^{18}\text{O}/^{16}\text{O}$  in meteoric waters. *Geochimica et*  
704 *Cosmochimica Acta*, 74(22): 6276-6286.

705 Luz, B., Barkan, E., Yam, R., Shemesh, A., 2009. Fractionation of oxygen and hydrogen isotopes in  
706 evaporating water. *Geochim. Cosmochim. Acta*, 73(22): 6697-6703.

707 Martín, J.L., Bethencourt, J., Cuevas-Agulló, E., 2012. Assessment of global warming on the island of  
708 Tenerife, Canary Islands (Spain). *Trends in minimum, maximum and mean temperatures since*  
709 *1944. Climatic Change*, 114(2): 343-355.

710 Meijer, H., Li, W., 1998. The use of electrolysis for accurate  $\delta^{17}\text{O}$  and  $\delta^{18}\text{O}$  isotope measurements in  
711 water. *Isotopes Environ. Health Studies*, 34(4): 349-369.

712 Merlivat, L., 1978. Molecular diffusivities of  $\text{H}_2^{16}\text{O}$ ,  $\text{HD}^{16}\text{O}$ , and  $\text{H}_2^{18}\text{O}$  in gases. *The Journal of Chemical*  
713 *Physics*, 69(6): 2864-2871.

714 Monteith, J., Unsworth, M., 2013. *Principles of environmental physics: plants, animals, and the*  
715 *atmosphere*. Academic Press.

716 Munné-Bosch, S., Alegre, L., 1999. Role of dew on the recovery of water-stressed *Melissa officinalis* L.  
717 plants. *J. Plant Physiol.*, 154(5-6): 759-766.

718 Nepstad, D.C., Stickler, C.M., Filho, B.S.-., Merry, F., 2008. Interactions among Amazon land use, forests  
719 and climate: prospects for a near-term forest tipping point. *Philos. T. R. Soc. B.*, 363(1498): 1737-  
720 1746.

721 Passey, B.H., Ji, H., 2019. Triple oxygen isotope signatures of evaporation in lake waters and carbonates:  
722 A case study from the western United States. *Earth Planet. Sci. Lett.*, 518: 1-12.

723 Qiao, N., Zhang, L., Huang, C., Jiao, W., Maggs-Kölling, G., Marais, E., Wang, L., 2020. Satellite observed  
724 positive impacts of fog on vegetation. *Geophys. Res. Lett.*: e2020GL088428.

725 Rahimi, J., Ebrahimpour, M., Khalili, A., 2013. Spatial changes of extended De Martonne climatic zones  
726 affected by climate change in Iran. *Theor. Appl. Climatol.*, 112(3-4): 409-418.

727 Rao, B., Liu, Y., Wang, W., Hu, C., Dunhai, L., Lan, S., 2009. Influence of dew on biomass and  
728 photosystem II activity of cyanobacterial crusts in the Hopq Desert, northwest China. *Soil*  
729 *Biology and Biochemistry*, 41(12): 2387-2393.

730 Ritter, F., Berkelhammer, M., Beysens, D., 2019. Dew frequency across the US from a network of in situ  
731 radiometers. *Hydrol. Earth Syst. Sc.*, 23(2): 1179-1197.

732 Rosenzweig, C., Abramopoulos, F., 1997. Land-surface model development for the GISS GCM. *J. Climate*,  
733 10(8): 2040-2054.

734 Schoenemann, S.W., Schauer, A.J., Steig, E.J., 2013. Measurement of SLAP2 and GISP  $\delta^{17}\text{O}$  and proposed  
735 VSMOW-SLAP normalization for  $\delta^{17}\text{O}$  and  $^{17}\text{O}$ -excess. *Rapid Commun. Mass Spectrom.*, 27(5):  
736 582-590.

737 Soderberg, K., Good, S.P., Wang, L., Caylor, K., 2012. Stable isotopes of water vapor in the vadose zone:  
738 A review of measurement and modeling techniques. *Vadose Zone Journal*, 11(3).

739 Steig, E., Gkinis, V., Schauer, A., Schoenemann, S., Samek, K., Hoffnagle, J., Dennis, K., Tan, S., 2014.  
740 Calibrated high-precision  $^{17}\text{O}$ -excess measurements using cavity ring-down spectroscopy with  
741 laser-current-tuned cavity resonance. *Atmos. Meas. Tech.*, 7(8): 2421-2435.

742 Surma, J., Assonov, S., Bolourchi, M., Staubwasser, M., 2015. Triple oxygen isotope signatures in  
743 evaporated water bodies from the Sistan Oasis, Iran. *Geophys. Res. Lett.*, 42(20): 8456-8462.

744 Surma, J., Assonov, S., Herwartz, D., Voigt, C., Staubwasser, M., 2018. The evolution of  $^{17}\text{O}$ -excess in  
745 surface water of the arid environment during recharge and evaporation. *Sci. Rep.*, 8(1): 4972.

746 Tian, C., Wang, L., 2019. Stable isotope variations of daily precipitation from 2014-2018 in the central  
747 United States. *Sci. Data*, 6: 190018.

748 Tian, C., Wang, L., Jiao, W., Li, F., Tian, F., Zhao, S., 2020. Triple isotope variations of monthly tap water  
749 in China. *Sci. Data*, 7(1): 1-6.

750 Tian, C., Wang, L., Kaseke, K.F., Bird, B.W., 2018. Stable isotope compositions ( $\delta^2\text{H}$ ,  $\delta^{18}\text{O}$  and  $\delta^{17}\text{O}$ ) of  
751 rainfall and snowfall in the central United States. *Sci. Rep.*, 8: 6712.

752 Tian, C., Wang, L., Novick, K.A., 2016. Water vapor  $\delta^2\text{H}$ ,  $\delta^{18}\text{O}$  and  $\delta^{17}\text{O}$  measurements using an off-axis  
753 integrated cavity output spectrometer-sensitivity to water vapor concentration, delta value and  
754 averaging-time. *Rapid Commun. Mass Spectrom.*, 30(19): 2077-2086.

755 Tian, C., Wang, L., Tian, F., Zhao, S., Jiao, W., 2019. Spatial and temporal variations of tap water  $^{17}\text{O}$ -  
756 excess in China. *Geochim. Cosmochim. Acta*: 1-14.

757 Tomaszkiwicz, M., Abou Najm, M., Beysens, D., Alameddine, I., El-Fadel, M., 2015. Dew as a sustainable  
758 non-conventional water resource: a critical review. *Environmental Reviews*, 23(4): 425-442.

759 Tomaszkiwicz, M., Najm, M.A., Beysens, D., Alameddine, I., Zeid, E.B., El-Fadel, M., 2016. Projected  
760 climate change impacts upon dew yield in the Mediterranean basin. *Sci.Total Environ.*, 566:  
761 1339-1348.

762 Tuller, S.E., Chilton, R., 1973. The role of dew in the seasonal moisture balance of a summer-dry climate.  
763 *Agricultural Meteorology*, 11: 135-142.

764 Uclés, O., Villagarcía, L., Cantón, Y., Lázaro, R., Domingo, F., 2015. Non-rainfall water inputs are  
765 controlled by aspect in a semiarid ecosystem. *Journal of Arid Environments*, 113: 43-50.

766 Uechi, Y., Uemura, R., 2019. Dominant influence of the humidity in the moisture source region on the  
767  $^{17}\text{O}$ -excess in precipitation on a subtropical island. *Earth Planet. Sci. Lett.*, 513: 20-28.

768 Uemura, R., Barkan, E., Abe, O., Luz, B., 2010. Triple isotope composition of oxygen in atmospheric water  
769 vapor. *Geophysical Research Letters*, 37(4).

770 Vuollekoski, H., Vogt, M., Sinclair, V.A., Duplissy, J., Järvinen, H., Kyrö, E.-M., Makkonen, R., Petäjä, T.,  
771 Prisle, N.L., Räisänen, P., 2015. Estimates of global dew collection potential on artificial surfaces.  
772 *Hydrol. Earth Syst. Sc.*(19): 601-613.

773 Wang, L., Caylor, K.K., Dragoni, D., 2009. On the calibration of continuous, high-precision  $\delta^{18}\text{O}$  and  $\delta^2\text{H}$   
774 measurements using an off-axis integrated cavity output spectrometer. *Rapid Commun. Mass*  
775 *Spectrom.*, 23(4): 530-536.

776 Wang, L., Kaseke, K.F., Ravi, S., Jiao, W., Mushi, R., Shuuya, T., Maggs-Kölling, G., 2019. Convergent  
777 vegetation fog and dew water use in the Namib Desert. *Ecohydrology*: e2130.

778 Wang, L., Kaseke, K.F., Seely, M.K., 2017. Effects of non-rainfall water inputs on ecosystem functions.  
779 *WIREs. Water*, 4(1): e1179.

780 Wang, S., Zhang, Q., 2011. Atmospheric physical characteristics of dew formation in semi-arid in loess  
781 plateau. *Acta. Phys. Sin.*, 60(5): 059203.

782 Wen, X., Lee, X., Sun, X., Wang, J., Hu, Z., Li, S., Yu, G., 2012. Dew water isotopic ratios and their  
783 relationships to ecosystem water pools and fluxes in a cropland and a grassland in China.  
784 *Oecologia*, 168(2): 549-561.

785 Wen, X., Zhang, S., Sun, X., Yu, G., Lee, X., 2010. Water vapor and precipitation isotope ratios in Beijing,  
786 China. *J. Geophys. Res.*, 115(D1).

787 Winkler, R., Landais, A., Sodemann, H., Dümbgen, L., Prié, F., Masson-Delmotte, V., Stenni, B., Jouzel, J.,  
788 2012. Deglaciation records of  $^{17}\text{O}$ -excess in East Antarctica: reliable reconstruction of oceanic  
789 normalized relative humidity from coastal sites. *Clim. Past*, 8(1): 1-16.

790 Winnick, M.J., Chamberlain, C.P., Caves, J.K., Welker, J.M., 2014. Quantifying the isotopic 'continental  
791 effect'. *Earth and Planetary Science Letters*, 406: 123-133.

792 Ye, Y., Zhou, K., Song, L., Jin, J., Peng, S., 2007. Dew amounts and its correlations with meteorological  
793 factors in urban landscapes of Guangzhou, China. *Atmospheric Research*, 86(1): 21-29.

794 Zhang, X., Yang, Z., Niu, G., Wang, X., 2009. Stable water isotope simulation in different reservoirs of  
795 Manaus, Brazil, by Community Land Model incorporating stable isotopic effect. *International*  
796 *Journal of Climatology: A Journal of the Royal Meteorological Society*, 29(5): 619-628.

797 Zhang, Y., Hao, X., Sun, H., Hua, D., Qin, J., 2019. How *Populus euphratica* utilizes dew in an extremely  
798 arid region. *Plant Soil*: 1-16.

799 Zhao, L., Xiao, H., Zhou, M., Cheng, G., Wang, L., Yin, L., Ren, J., 2012. Factors controlling spatial and  
800 seasonal distributions of precipitation  $\delta^{18}\text{O}$  in China. *Hydrological Processes*, 26(1): 143-152.

801

**Table 1. The detailed information of the three studied sites under different climate settings.**

Site	Country	Latitude (°)	Longitude (°)	Elevation (m, a.s.l)	Mean annual temperature (°C)	Mean annual relative humidity (%)	Precipitation (mm)	Aridity index	Köppen climate classification
Gobabeb Research and Training Center	Namibia	-23.55	15.04	405	21.1	50	<20	0.01	Desert climate
Nice	France	43.74	7.27	310	16.0	78	733	0.98	Mediterranean climate
Indianapolis	United States	39.88	-86.27	258	10.2	69	953	0.96	Humid continental climate

**Table 2. The variables and parameters of optimal evaporation models under non-steady state conditions for the dew samples in Gobabeb and Indianapolis. For Indianapolis, the samples are the ones with temperature over 14.7°C.**

Variable or parameter	Dew in Gobabeb	Dew <sub>T≥14.7°C</sub> in Indianapolis
$\delta^{18}\text{O}$ of initial water	-6.771	-9.164
$\delta^2\text{H}$ of initial water	-27.708	-56.232
$\delta^{17}\text{O}$ of initial water	-3.552	-4.813
f	0.5	0.7
$^{18}\alpha_{\text{eq}}$	1.01055	1.01001
$^2\alpha_{\text{eq}}$	1.09455	1.08745
$^{17}\alpha_{\text{eq}}$	1.00557	1.00528
$^{18}\alpha_{\text{diff}}$	1.02830	1.02830
$^2\alpha_{\text{diff}}$	1.02486	1.02486
$^{17}\alpha_{\text{diff}}$	1.01456	1.01456
Average nocturnal temperature	11.8	17.4
Average nocturnal relative humidity	78	93
Simulated relative humidity	78	98
Average daily temperature	18.6	19.2
$^{18}\alpha_{\text{l/v}}$	1.00990	1.00985
$^2\alpha_{\text{l/v}}$	1.08600	1.08529
$^{17}\alpha_{\text{l/v}}$	1.00523	1.00520
$\delta^{18}\text{O}$ of precipitation	-3.533	-5.248
$\delta^2\text{H}$ of precipitation	-25.743	-33.791
$\delta^{17}\text{O}$ of precipitation	-1.857	-2.745
$\delta^{18}\text{O}$ of atmospheric water vapor	-13.305	-14.950
$\delta^2\text{H}$ of atmospheric water vapor	-102.898	-109.725
$\delta^{17}\text{O}$ of atmospheric water vapor	-7.047	-7.902
$\delta^{17}\text{O}$ -excess of atmospheric water vapor	0	20

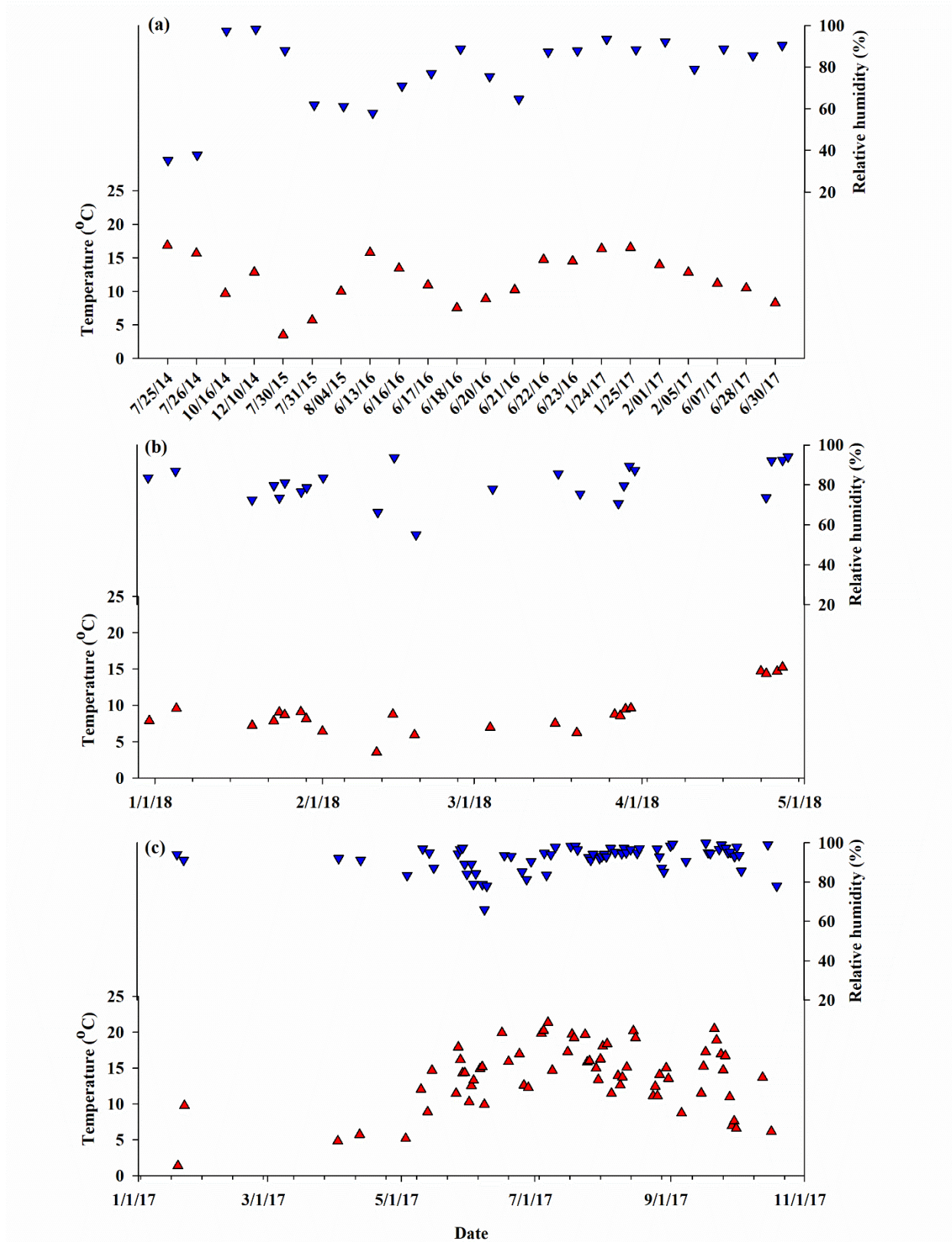
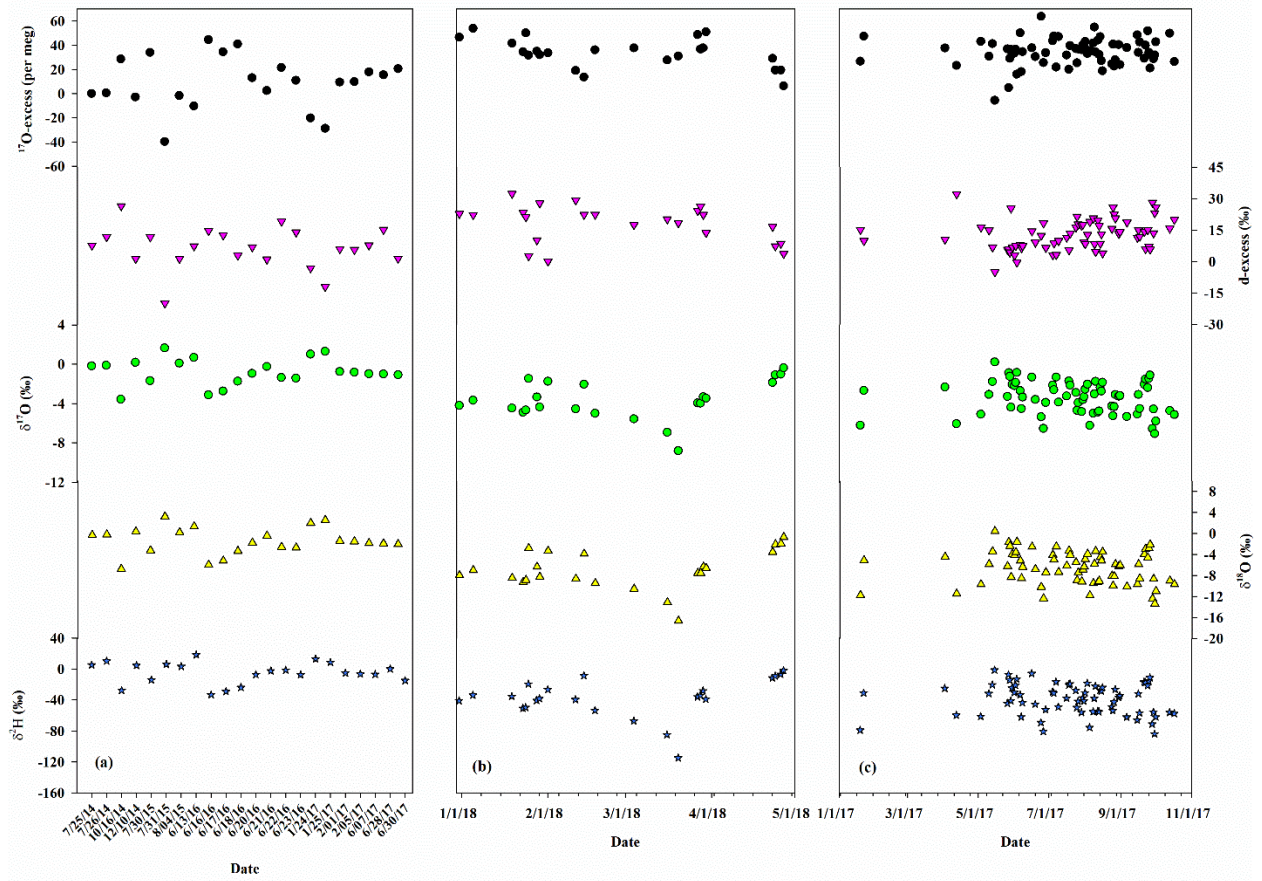


Figure 1. Daily nocturnal average temperature and relatively humidity at Gobabeb (a), Nice (b), and Indianapolis (c).



**Figure 2. Dew stable isotope variations at Gobabeb (a), Nice (b), and Indianapolis (c). From top to bottom:  $^{17}\text{O}$ -excess,  $d$ -excess,  $\delta^{17}\text{O}$ ,  $\delta^{18}\text{O}$ , and  $\delta^2\text{H}$ .**

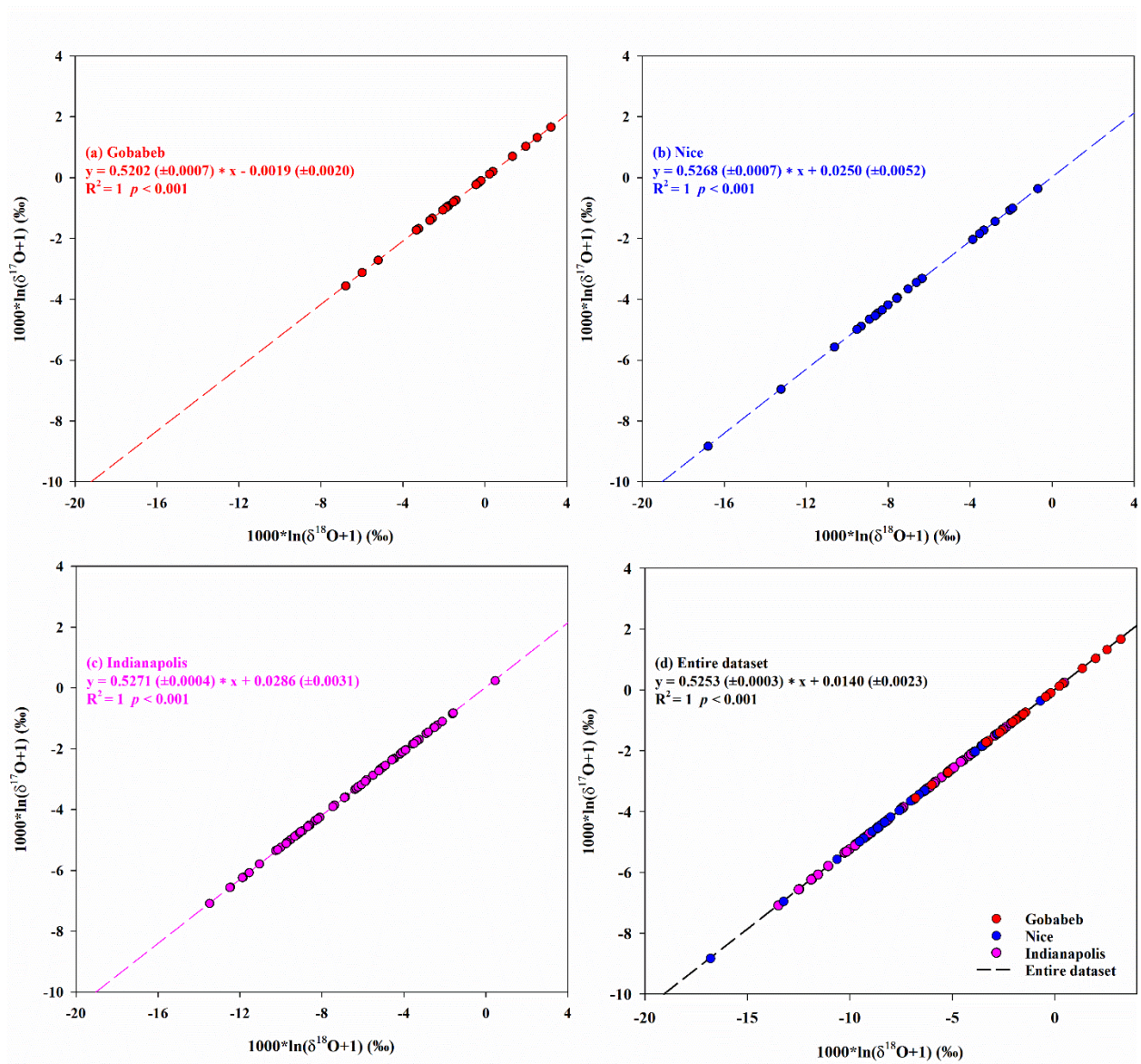
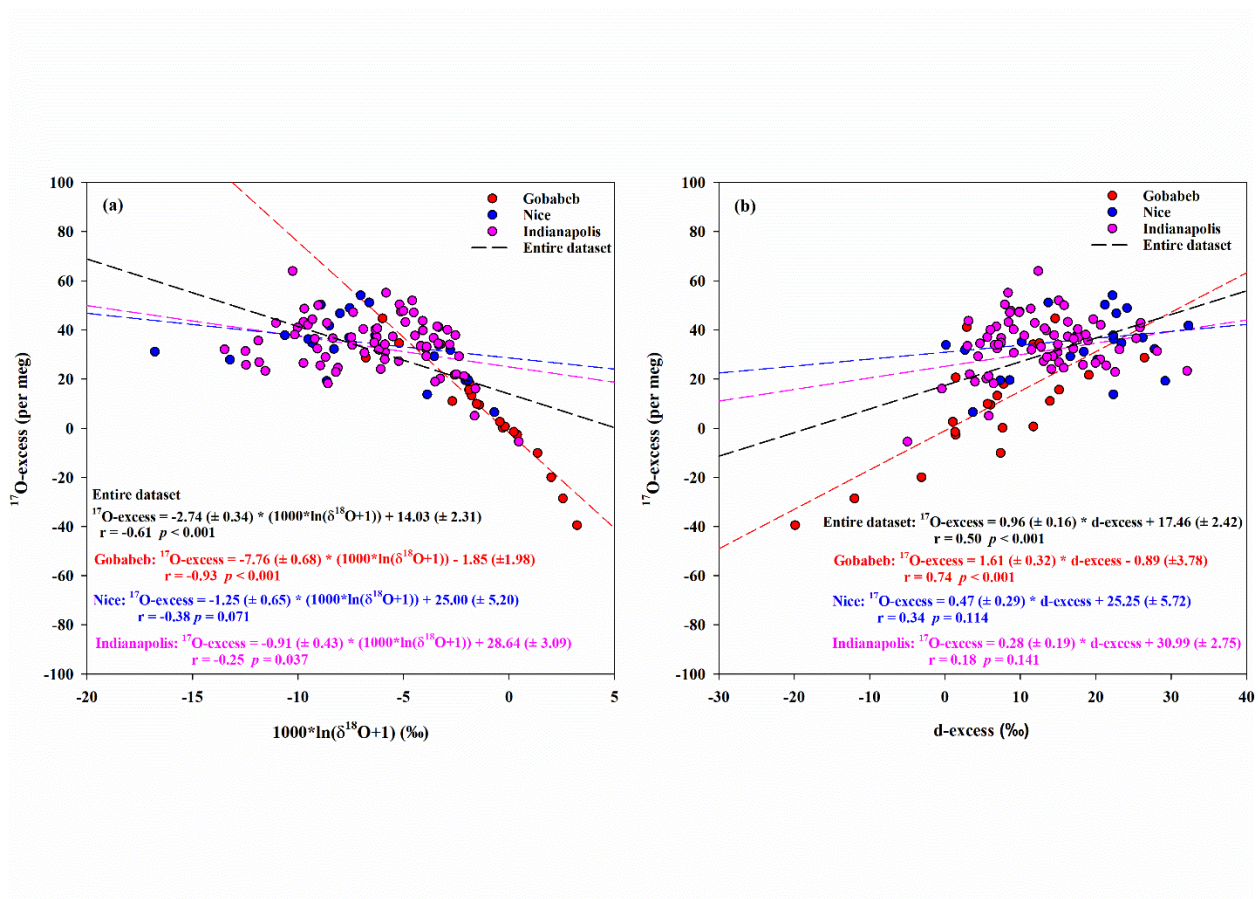


Figure 3. The relationships between  $\delta^{17}\text{O}$  and  $\delta^{18}\text{O}$  based on daily dew at Gobabeb (a), Nice (b), Indianapolis (c), and all of the three sites (d).



**Figure 4.** The relationships between  $^{17}\text{O-excess}$  and both  $\delta^{18}\text{O}$  (a) and d-excess (b) based on daily dew at Gobabeb, Nice, and Indianapolis.

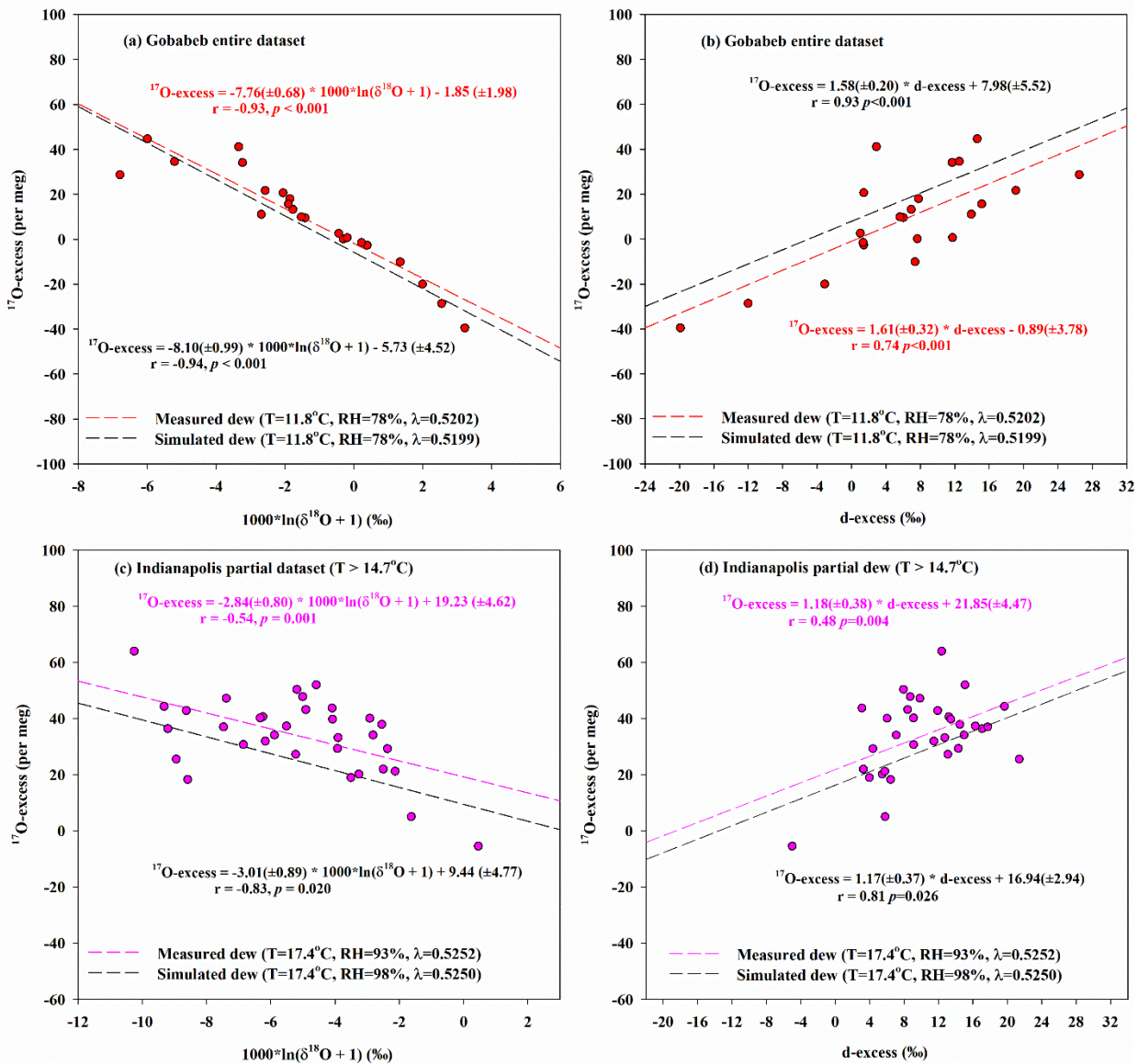
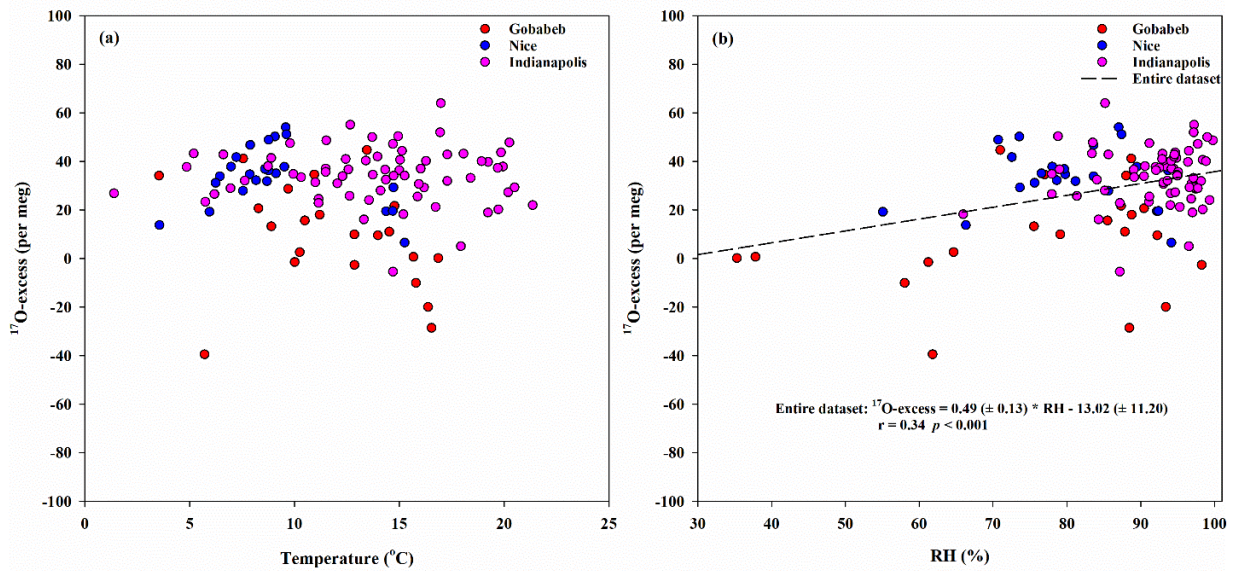
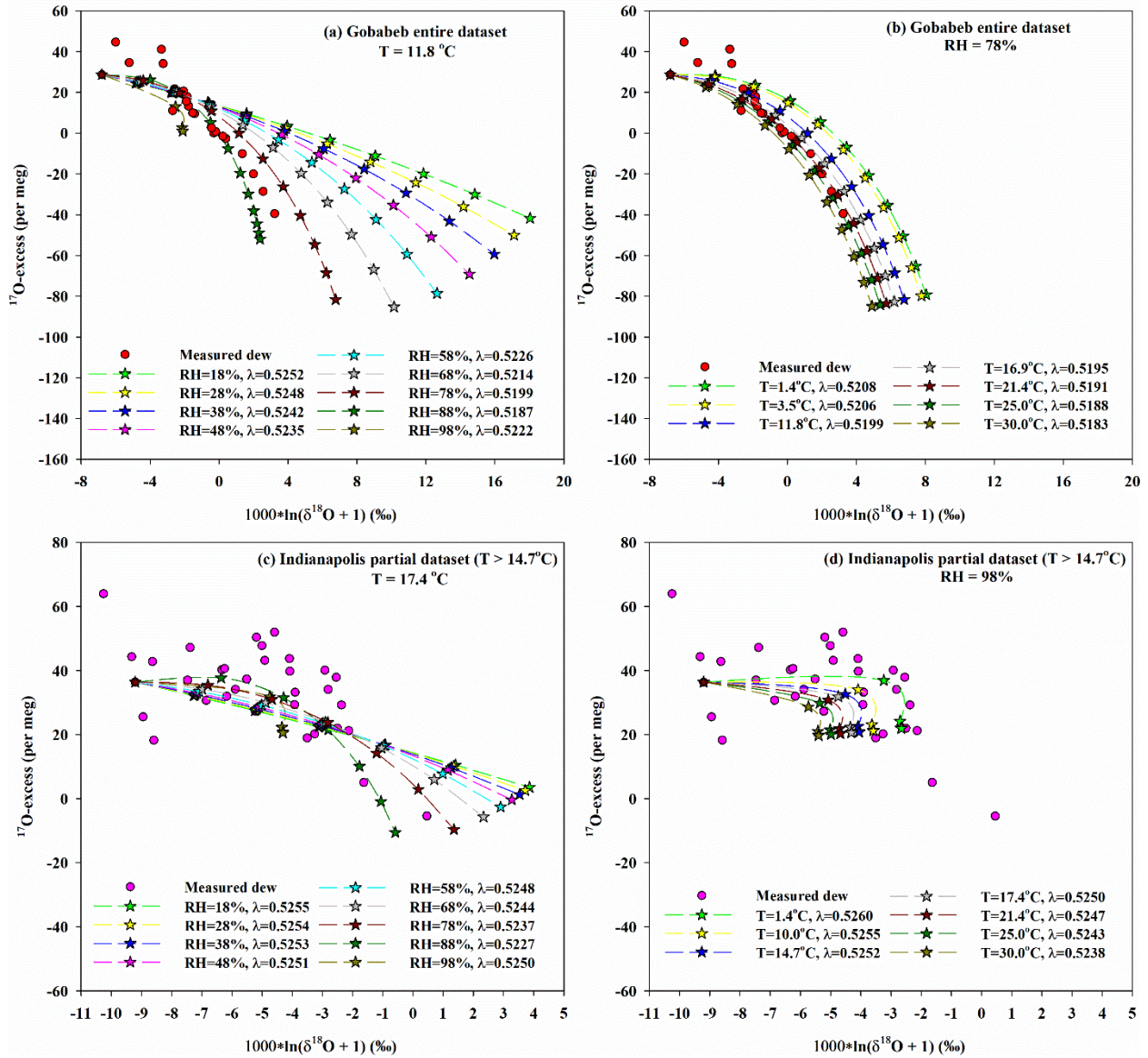


Figure 5. Modeled isotopic evolution of different sources at Gobabeb (a-b), and Indianapolis (c-d) in comparison to measured dew isotopic compositions.



**Figure 6. The relationships between  $^{17}\text{O}$ -excess and both temperature (a) and relative humidity (b) based on daily dew at Gobabeb, Nice, and Indianapolis.**



**Figure 7. Modeled isotopic values (star) in Gobabeb and Indianapolis under different temperature and relative humidity in comparison to measured dew isotopic compositions (circle).**